

UC Berkeley

UC Berkeley Previously Published Works

Title

Mechanism and Kinetics of Isobutene Formation from Ethanol and Acetone over $Zn_xZr_yO_z$

Permalink

<https://escholarship.org/uc/item/22w352c4>

Journal

ACS Catalysis, 9(12)

ISSN

2155-5435

Authors

Rorrer, Julie E
Toste, F Dean
Bell, Alexis T

Publication Date

2019-12-06

DOI

10.1021/acscatal.9b03045

Peer reviewed

Mechanism and Kinetics of Isobutene Formation from Ethanol and Acetone over $Zn_xZr_yO_z$

Julie E. Rorrer,^{†,§} F. Dean Toste,^{‡,§} and Alexis T. Bell^{*,‡,§}

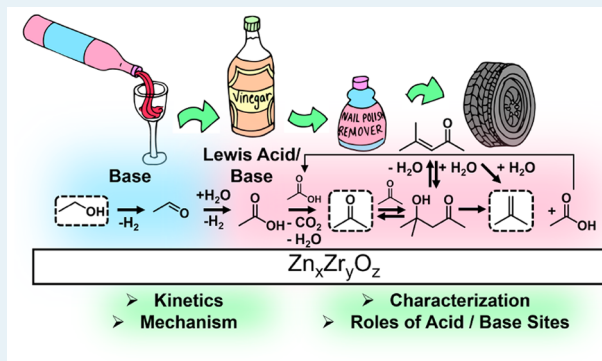
[†]Department of Chemical and Biomolecular Engineering and [‡]Department of Chemistry, University of California Berkeley, Berkeley, California 94720, United States

[§]Chemical Sciences Division, Lawrence Berkeley National Laboratory, Berkeley, California 94720, United States

Supporting Information

ABSTRACT: Isobutene is a specialty chemical used in the production of fuel additives, polymers, and other high-value products. While normally produced by steam cracking of petroleum naphtha, there is increasing interest in identifying routes to synthesizing isobutene from biomass-derived compounds, such as ethanol and acetone. Recent work has shown that zinc–zirconium mixed oxides are effective and selective catalysts for producing isobutene from ethanol. However, the reaction pathway, the roles of acidic and basic sites, and the role of water in promoting stability and selectivity are not yet clearly defined. In this study, a series of zinc–zirconium mixed oxides with tunable acid–base properties were synthesized and characterized with XRD, Raman spectroscopy, BET, CO_2 -TPD, NH_3 -TPD, and IR DRIFTS of adsorbed pyridine in order to probe the roles of acid and base sites for each step in the ethanol-to-isobutene reaction pathway. The observed reaction kinetics, supported by modeling of these kinetics, suggest that the reaction of ethanol to isobutene proceeds via a five-step sequence. Ethanol first undergoes dehydrogenation to acetaldehyde, which is then oxidized to acetic acid. This product undergoes ketonization to produce acetone, which dimerizes to form diacetone alcohol. The latter product either decomposes directly to isobutene and acetic acid or produces these products by dehydration to mesityl oxide and subsequent hydrolysis. The acetic acid formed undergoes ketonization to produce additional acetone. The dispersion of zinc oxide on zirconia was found to produce a balance between Lewis acidic and basic sites that prevent the loss of ethanol via dehydration to ethylene and promote the cascade reactions of ethanol and acetone to isobutene. Water, while inhibiting both isobutene and mesityl oxide formation, improves isobutene selectivity by suppressing side reactions such as unimolecular dehydration, acetone decomposition, and deactivation due to coke formation.

KEYWORDS: isobutene, ethanol, acetone, ketonization, aldol condensation, metal oxides, zinc, zirconium



1. INTRODUCTION

Isobutene is a valuable platform molecule used for the synthesis of polymers, such as butyl rubber, and other polymer precursors, such as methyl methacrylate, methacrolein, and acrylics.¹ Ethers such as methyl-*tert*-butyl ether (MTBE) and ethyl-*tert*-butyl ether (ETBE), high-octane additives for gasoline, can be produced by reaction of isobutene with an alcohol.^{2,3} The principal source of isobutene today is steam cracking of naphtha, dehydration of fossil-derived *tert*-butanol, or dehydrogenation of petroleum-derived isobutane.⁴ Isobutene can also be produced via the reaction of CO and H_2 , obtained by steam reforming of methane, over a zirconia-based catalyst in a process known as isosynthesis.^{5–8} Growing concern with the rise in atmospheric CO_2 levels caused by the consumption of petroleum-derived sources of carbon has motivated exploration of renewable sources of carbon to meet the increasing global demand for fuels and specialty chemicals.^{9,10} Fermentation of monosaccharides to produce

renewable isobutene has been demonstrated although the yields and cost are not yet competitive with fossil fuel-based production of isobutene.¹¹

Ethanol and acetone are attractive starting points for the synthesis of isobutene since both can be produced by the fermentation of biomass-derived sugars.^{12–14} Recent work by Sun et al. has demonstrated that ethanol and acetone can be converted into isobutene with high selectivity over zinc–zirconia mixed oxide catalysts.^{15–17} The authors identified $Zn_1Zr_{10}O_z$ as a selective and stable catalyst for the production of isobutene from ethanol and acetone in the gas phase at 723 K with a steam-to-carbon molar ratio of 5. The conversion of acetone to isobutene was thought to proceed via the adsorption of acetone on a Lewis acidic Zr atom followed by

Received: July 18, 2019

Revised: October 9, 2019

Published: October 10, 2019

hydrogen extraction by a basic oxygen to form an adsorbed enolate, which then attacks a second acetone to form diacetone alcohol. This product then either decomposes to form isobutene and acetic acid or dehydrates to form mesityl oxide, which then hydrolyzes to produce isobutene and acetic acid.¹⁶ Subsequent work by Li et al. showed that diacetone alcohol, mesityl oxide, phorone, and isophorone are potential intermediates in the conversion of acetone to isobutene over $Zn_xZr_yO_z$.¹⁸ Crisci et al. have also reported that isobutene yields of up to 50% could be obtained by reacting acetic acid over an amorphous binary metal oxide ($Zn_2Zr_8O_z$) at 723 K.¹⁹ We note that while potential intermediates have been identified for the reaction of acetone to isobutene over $Zn_xZr_yO_z$, the mechanism is not yet clearly defined. For the reaction of ethanol to isobutene, neither the reaction pathway nor the active sites necessary for each step in the reaction pathway are known.

Sun et al. suggested that a balance between acid and base sites on $Zn_xZr_yO_z$ is responsible for the effective cascade reaction of bioethanol and acetone to isobutene.¹⁵ The authors observed a selectivity to isobutene of over 88% from acetone at 723 K in the presence of water over $Zn_1Zr_{10}O_z$.¹⁶ By contrast, ZrO_2 exhibited a significantly lower selectivity to isobutene (~13%) for the reaction of acetone, with methane and CO_2 (~60 and ~27%, respectively) appearing as the principal products. It was suggested that the zinc oxide present on the surface passivates the strong Brønsted acidity of the zirconia and introduces basicity, preventing decomposition of acetone as well as suppressing ethanol dehydration to ethylene for the ethanol to isobutene reaction. These authors also found that the selectivity toward isobutene from acetone over pure ZnO was approximately the same (~80%) as that observed over $Zn_1Zr_{10}O_z$ for an acetone conversion of ~28%. While the comparison of ZrO_2 and $Zn_1Zr_{10}O_z$ suggests that basicity is necessary for the reactions of ethanol and acetone to isobutene, the role of the zirconia support remains unclear. Because only a small difference in isobutene selectivity is observed for the reaction of acetone over ZnO compared to $Zn_1Zr_{10}O_z$ at the same conversion, it is unclear what role the balance between acid and base properties of the catalyst plays in the acetone to isobutene reaction.

The role of Brønsted acid sites in the synthesis of isobutene has also been considered. Herrmann and Iglesia have recently reported the selective conversion of acetone to isobutene and acetic acid over Brønsted acidic aluminosilicates and proposed a radical-mediated pathway for the formation of isobutene via an equilibrated pool of C_6 intermediates; however, the catalyst underwent rapid deactivation due to side product formation over the Brønsted acid sites, which produced coke.²⁰ Hutchings et al. have also observed catalyst deactivation for the reaction of acetone to isobutene over Brønsted acidic zeolites BEA and ZSM-5.²¹ Ponomareva et al. have suggested that Brønsted acid sites on cesium-modified mordenite and MCM-41 were preferable for the synthesis of isobutene from acetone although these authors also observed catalyst deactivation due to coking.²² Sun et al. and Liu et al. have suggested that weak Brønsted acid sites are responsible for isobutene formation, but strong Brønsted acid sites catalyze coke formation and that the absence of Brønsted acidity prevents side reactions.^{16,17} Crisci et al. have noted that Brønsted acid sites may be required to promote the hydrolysis of mesityl oxide to isobutene and that ZnO is unable to catalyze the formation of isobutene from acetic acid.¹⁹

Therefore, examination of the literature does not fully address the question of which active sites are necessary for isobutene formation from ethanol and acetone. While the dispersion of ZnO on zirconia provides basicity and suppresses ethanol dehydration, it is unclear whether zirconia simply provides a high surface area support or whether the interaction of the dispersed ZnO with the support produces additional or stronger Lewis acidity, or aids in the formation of oxygen vacancies that promote the dissociation of water. The aim of this work was to develop a detailed understanding of the sequence of reactions involved in the conversion of ethanol and acetone to isobutene over $Zn_xZr_yO_z$. This effort involved identifying the stable reaction intermediates and the types of sites required to promote each phase of the reaction sequence. To this end, we synthesized and characterized a series of $Zn_xZr_yO_z$ catalysts with varying acidity and basicity and used these materials in a systematic study of the roles of acid and base sites for each step in the reaction pathway. The presentation of our results starts by detailing the catalyst characterization. We then develop a picture for the overall reaction pathway involved in the conversion of ethanol and acetone to isobutene over $Zn_xZr_yO_z$. Next, we propose a mechanism for each step in the reaction pathway that is consistent with the experimental data, catalyst characteristics, and a thorough review of the existing literature. Finally, we discuss the role of water in promoting isobutene formation and preventing catalyst deactivation as well as the role of the mesityl oxide intermediate.

2. MATERIALS AND METHODS

2.1. Materials. All chemicals obtained commercially were used without further purification. The following compounds were obtained from Sigma Aldrich: ethanol (>99.5%), 4-hydroxy-4-methyl-2-pentanone (diacetone alcohol, 99%), mesityl oxide (90%, remainder 4-methyl-4-penten-2-one), acetaldehyde solution (50 wt % in ethanol), acetone (>99.5%), acetic acid (>99%), diethyl ether (>99%), and ethyl acetate (99.8%). Acetone- d_6 (99.9%) and deuterium oxide (99.9%) were obtained from Cambridge Isotope Laboratories. Standard gas (3.01% methane, 1.5% ethylene, 1.5% ethane, 1% propene, 1.01% propane, 0.745% *cis*-2-butene, 0.748% *trans*-2-butene, 0.75% butane, 0.6% *n*-pentane in He), 1% Ar in He (CSG), ammonia (99.995%), and He (5.0 UHP) were obtained from Praxair. Isobutene gas (99%) was obtained from Sigma-Aldrich. Nanopure water was obtained via a MilliQ water purification system. Zinc oxide (99.9995% metals basis) was obtained from Puratronic.

2.2. Synthesis of Zirconia and Zinc–Zirconia Mixed Oxide. Porous amorphous zirconia and the zinc–zirconia mixed oxides were synthesized using modifications of previously reported methods.^{16,23–26} Amorphous zirconium oxyhydroxide ($ZrO_x(OH)_{4-2x}$) was formed by adding ammonium hydroxide (Spectrum, 28–30%) dropwise to a stirred solution of 0.5 M zirconyl chloride octahydrate (Sigma Aldrich, 98%) at 298 K. The precipitate was filtered and rinsed with 10% ammonium hydroxide and dried at 383 K for 24 h. The zinc–zirconia mixed oxides were prepared via incipient wetness impregnation of amorphous zirconium oxyhydroxide with an aqueous solution of zinc nitrate hexahydrate (Alfa Aesar, 99%) in a mortar with varying concentrations of zinc nitrate corresponding to the target Zn weight loadings. The wetted support was ground with a mortar and pestle. After impregnation, the catalyst was dried at 383 K for 0.3 h, then

heated in air at 3 K min^{-1} to a temperature of 673 K, and held at this temperature for 2 h. This step was followed by further heating the catalyst to 823 K at a rate of 5 K min^{-1} and holding it at this temperature for 3 h after which it was cooled to room temperature. Monoclinic zirconia was prepared using the same calcination procedure but in the absence of the zinc precursor.

2.3. Catalyst Characterization. Powder X-ray diffraction (XRD) patterns for ZnO, ZrO₂, and the Zn_xZr_yO_z catalysts were taken with a Bruker D8 GADDS diffractometer equipped with a Cu K α source (40 kV, 40 mA). Raman spectra were obtained with a LabRAM HR Horiba Scientific Raman spectrometer equipped with a 532 nm^{-1} laser. BET surface areas were calculated from nitrogen adsorption isotherms acquired with a Micrometrics Gemini VII surface area and porosity instrument after being degassed overnight at 393 K with a Micrometrics VacPrep 061. Scanning electron microscopy images of Zn_xZr_yO_z (2.2 wt % Zn) were acquired with an FEI Quanta FEG 250 scanning electron microscope (SEM) equipped with a Bruker Quantax energy-dispersive spectrometer (EDS). ICP elemental analysis was performed by Galbraith Laboratories, Inc. to determine Zn and Zr loadings.

The identification of Brønsted and Lewis acid sites was determined from IR spectra of adsorbed pyridine. Spectra were acquired using a Thermo Scientific Nicolet 6700 Fourier transform infrared (FT-IR) spectrometer equipped with a diffuse reflectance infrared Fourier transform spectroscopy (DRIFTS) cell. A mixture of catalyst (50 mg) diluted with KBr (250 mg) was added to the DRIFTS cell and pre-treated at 573 K for 2 h under 50 mL min^{-1} helium. DRIFTS scans for ZnO were repeated in the presence and absence of a KBr diluent. Background scans of the catalysts were taken at 393, 423, 473, 523, and 573 K. Pyridine (2 μL) was introduced into the He flow at 323 K, and spectral data was taken after stabilization of adsorbed pyridine at 323 K. The temperature was then raised to measure the amount of pyridine that remained adsorbed at 373, 393, 423, 473, 523, and 573 K. Spectral intensities were calculated using the Kubelka–Munk function.

The density of acid sites was measured by ammonia temperature-programmed desorption (NH₃-TPD).²⁷ NH₃-TPD profiles of the ZnO, ZrO₂, and Zn_xZr_yO_z samples were acquired using a gas-phase flow reactor with an outlet flowing to a mass spectrometer (MKS, Cirrus). Samples (~200 mg) were loaded into a quartz reactor and plugged on either end with quartz wool. A thermocouple was placed above the catalyst bed. Samples were first heated at 5 K min^{-1} to a temperature of 723 K and held for 0.5 h in a flow of 50 mL min^{-1} He (Praxair, UHP). The reactor was then cooled to 323 K, the He flow was increased to 250 mL min^{-1} , and 1% Ar in He (Praxair, CSG) was introduced at 50 mL min^{-1} . The catalyst was saturated with NH₃ by flowing 5 mL min^{-1} of NH₃ for 0.5 h. After stopping the flow of NH₃, 300 mL min^{-1} of He was passed over the catalyst bed overnight to remove any physisorbed NH₃ from the catalyst surface. The temperature-programmed desorption was carried out in 50 mL min^{-1} of 1% Ar in He as the temperature was ramped from 323 to 973 K at a ramp rate of 5 K min^{-1} . The desorbed NH₃ coming out of the outlet flow was directed to the mass spectrometer for quantification. Standards with known concentrations of NH₃ were taken before and after each TPD measurement to account for any drift during the course of the experiment. Ar was used as an internal standard for quantification. The quantity of acid sites on the catalyst surface corresponds to the amount of NH₃ desorbed from the catalyst during the TPD.

The density of basic sites was measured by temperature-programmed desorption of CO₂ (CO₂-TPD) using a Micro-metrics Auto Chem II 2920 instrument equipped with a thermal conductivity detector. The catalyst samples were pretreated under He flow at 873 K for 3 h and then cooled to 313 K. CO₂ was then introduced at 313 K for 0.5 h at 30 mL min^{-1} and then purged with He at 313 K for 0.5 h to remove any physisorbed species from the surface. The temperature-programmed desorption of CO₂ was then performed in 50 mL min^{-1} He using a temperature ramp rate of 5 K min^{-1} up to a temperature of 1073 K.

2.4. Reactions. Gas-phase reactions were performed in a gas-phase flow reactor. The catalyst was placed in a 6.35 mm-OD quartz tube with an expanded section (~12.7 mm OD, ~20 mm length) packed with quartz wool above and below the catalyst. The reactor temperature was maintained using a tube furnace equipped with an Omega temperature controller and a K-type thermocouple. Prior to each reaction, the catalyst was treated in 40 mL min^{-1} He for 2 h at 723 K at a ramp rate of 10 K min^{-1} . The same catalyst surface area was used to study reactions over Zn_xZr_yO_z and ZnO in order to compare activity and selectivity at similar reactant conversions.

Reactions were performed using helium (Praxair, 5.0 Ultra High Purity) as a carrier gas. Liquid-phase reactants (ethanol, acetaldehyde/ethanol solution, acetic acid, acetone, diacetone alcohol, mesityl oxide, and nanopure water) were injected via a Cole Palmer 74900 series syringe pump into the reactor with lines heated to $>367\text{ K}$ to vaporize the liquids before reaching the reactor. Experiments were carried out at atmospheric pressure, between 573 and 823 K, with total flow rates ranging from 10 to 300 mL min^{-1} in a balance of helium. Reaction products were analyzed using an Agilent 6890 N gas chromatograph (GC) containing a (5%-phenyl)-methylpolysiloxane capillary column (Agilent, HP-5) connected to a flame ionization detector. The temperature program for the GC column began at 263 K (cooled with liquid N₂), then ramped to 283 K at 3 K min^{-1} , then ramped to 353 K at 33 K min^{-1} , held at 353 K for 1 min, then ramped to 363 K at 33 K min^{-1} , and held at 363 K for 1 min. Retention times and response factors were obtained either by injecting solutions of products via the syringe pump or by flowing standard gas mixtures into the reactor. Concentrations of CO₂ were estimated based on the stoichiometry shown in Section 3.2, closing carbon balances to within $\pm 5\%$. Response factors for higher olefins (C₉+), produced in the absence of water, were estimated using the effective carbon number method.²⁸

3. RESULTS AND DISCUSSION

3.1. Catalyst Characterization. To probe the relationship between Lewis acidity and basicity and catalytic activity for the ethanol to isobutene reaction, Zn_xZr_yO_z compounds with different weight loadings of Zn were synthesized and characterized using a variety of structural and surface characterization techniques. This series of catalysts was then used to identify the effects of acidity and basicity on the kinetics and mechanism of the ethanol and acetone to isobutene reactions. The Zn weight loadings, BET surface areas, identification and quantification of acid sites, and quantification of basic sites are summarized in Table 1. Apart from the low-surface-area ZnO, the weight loading of Zn had a minimal effect on the surface area of the catalysts, which were all within the range of $46\text{--}56\text{ m}^2\text{ g}^{-1}$. The weight loadings of Zn in the bulk measured by ICP closely matched

Table 1. Summary of Catalyst Characteristics

catalyst	wt % Zn ^a	BET surface area (m ² g ⁻¹)	basicity ^b (μmol CO ₂ /m ²)	acidity ^c (μmol NH ₃ /m ²)
WZ-ZnO	80.3	3.6	4.78	1.9
Zn _x Zr _y O _z	8.0	53.3	2.81	2.6
Zn _x Zr _y O _z	3.8	46.1	2.43	1.8
Zn _x Zr _y O _z	2.7	48.1	2.51	1.5
Zn _x Zr _y O _z	2.2	51.0	3.21	2.6
Zn _x Zr _y O _z	1.7	49.5	2.75	2.2
Zn _x Zr _y O _z	1.6	48.1	2.65	2.2
m-ZrO ₂	0	55.7	1.83	2.6

^aWeight percent zinc measured by ICP by Galbraith. ^bMeasured from CO₂ TPD. ^cMeasured from NH₃ TPD.

the targeted amounts of Zn added to the support via incipient wetness impregnation (Figure S1).

X-ray diffraction (XRD) and Raman spectroscopy were used as complementary techniques to identify phase transformations of the zirconia support that occurred with increasing zinc loading. The XRD patterns and Raman spectra are shown in Figure 1a, b. Figure 1a shows that the dominant phase of the pure zirconia is monoclinic, as evidenced by the peaks at 2θ angles of 24, 28, 32, and 56°, ^{29–31} denoted by stars. As the Zn loading increases, prominent peaks at 2θ angles of 30, 35, 50, and 59° appear, denoted by triangles, that are characteristic of tetragonal zirconia. ^{30–32} The pure bulk ZnO exhibits peaks at 2θ angles of 32, 34, 37, 47, 57, 64, 67, 68, and 69°, denoted by the squares, that are characteristic of wurtzite (WZ). ^{33,34} The wurtzite phase is not observed for Zn_xZr_yO_z, suggesting that clusters of bulk ZnO are not present on the surface of these catalysts. As the weight loading of Zn approaches a theoretical monolayer coverage of zinc oxide over the zirconia (occurring at molar ratio of Zn/Zr ~1:50 for particles 5 μm in diameter), the crystal structure of the zirconia changes from monoclinic to tetragonal. This suggests that the incorporation of Zn into the oxide structure stabilizes the tetragonal phase of zirconia. We

have previously observed this stabilizing effect for tungstated zirconia; as tungsten oxide is added to the surface of zirconia, the Zr–O–W interactions stabilize the tetragonal zirconia phase and inhibit the sintering of zirconia to the more thermodynamically stable monoclinic phase. ²⁴ Similarly, the absence of the wurtzite phase suggests that Zr–O–Zn interactions are present instead of clusters of ZnO.

Because the weight loadings of Zn are low, XRD may not be sufficient to identify the presence or absence of the wurtzite phase of ZnO; therefore, Raman spectra of the series of catalysts were acquired to provide further evidence for the absence of wurtzite ZnO, as shown in Figure 1b. Raman spectroscopy is sensitive to the wurtzite phase of ZnO, as evidenced by the strong band at approximately 430 cm⁻¹. ^{33,35} Consistent with the observed changes in the XRD pattern, Raman spectroscopy shows that the monoclinic phase of zirconia gives way to the tetragonal phase as Zn is added to the zirconia. This change in phase is evidenced by the decrease in intensity of the Raman bands at 181, 377, 472, 556, 616, and 634 cm⁻¹ (monoclinic phase) as Zn loading increases and the increase in intensity of the bands at 149, 269, and 312 cm⁻¹ (tetragonal phase) as the Zn loading increases. ^{36–38} No evidence for a band at 430 cm⁻¹ was observed for any of the Zn_xZr_yO_z catalysts, further indicating the absence of ZnO on the catalyst surface. SEM–EDX characterization of Zn_xZr_yO_z with 2.2 wt % Zn supports the conclusion that Zn is well dispersed on the surface of the catalyst, as shown in Figure 1d. The trends in XRD patterns and Raman spectra are in good agreement with the work of Baylon et al., who found that with increasing Zn loading, the fraction of tetragonal versus monoclinic zirconia in Zn_xZr_yO_z increases and that ZnO is not present. ³⁶ These authors also found that for intermediate weight loadings of Zn, the formation of Zn–O–Zr moieties with balanced acid–base properties facilitated cascade aldolization and self-deoxygenation reactions of acetone and methyl ethyl ketone. ³⁶

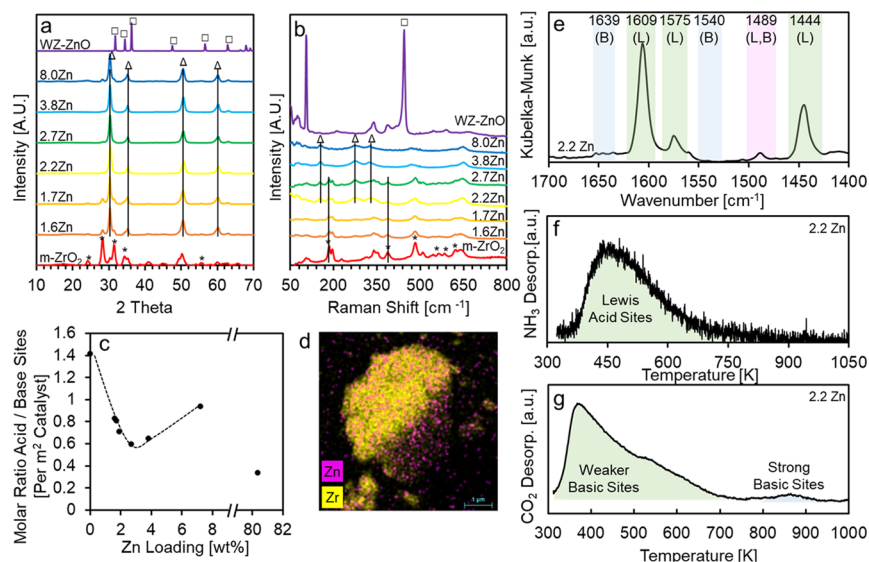


Figure 1. (a) X-ray diffraction patterns of ZnO, ZrO₂, and Zn_xZr_yO_z catalysts for different weight loadings of Zn (1.6–8.0 wt %); (b) Raman spectra of catalysts – abbreviations wurtzite (WZ), monoclinic (m); symbols: wurtzite phase (squares), tetragonal zirconia (triangles), monoclinic zirconia (stars); (c) molar ratio of total Lewis acid to base sites as a function of the weight loading of Zn; (d) SEM EDX of Zn_xZr_yO_z (2.2 wt % Zn); (e) Representative DRIFTS spectrum of pyridine adsorbed to Zn_xZr_yO_z (2.2 wt % Zn) at 393 K (intensities normalized by the Kubelka–Munk function); (f) NH₃-TPD profile for Zn_xZr_yO_z (2.2 wt % Zn); (g) CO₂-TPD profile for Zn_xZr_yO_z (2.2 wt % Zn).

A combination of diffuse reflectance infrared spectroscopy of adsorbed pyridine (DRIFTS-py), ammonia temperature-programmed desorption (NH₃-TPD), and CO₂ temperature-programmed desorption (CO₂-TPD) was used to identify and quantify the acid and base sites on the catalysts. A representative DRIFTS spectrum for the adsorption of pyridine onto the Zn_xZr_yO_z catalyst with 2.2 wt % Zn at 393 K is shown in Figure 1e. Bands at 1609, 1575, and 1444 cm⁻¹ are characteristic of pyridine adsorbed on Lewis acid sites; however, the absence of bands at 1639 and 1540 cm⁻¹, corresponding to the pyridinium ion, suggests that there are no Brønsted acid sites present.^{30,39} DRIFTS-py spectra for ZnO, ZrO₂, and Zn_xZr_yO_z samples with Zn weight loadings of 1.6–8.0% are shown in Figure S2. For each of these catalysts, including monoclinic ZrO₂, Lewis acid sites were observed but none of the catalysts contained significant Brønsted acid sites.

NH₃-TPD was used to quantify the concentration of acid sites. A representative NH₃-TPD profile for the Zn_xZr_yO_z catalyst with 2.2 wt % Zn is shown in Figure 1f, and the areal concentrations of adsorbed ammonia in units of μmol NH₃/m² of catalyst surface area are summarized in Table 1. The shaded green region in Figure 1f represents NH₃ desorption from both weak and strong Lewis acid sites. The NH₃-TPD profiles for the full series of catalysts are shown in Figure S3a. Generally, the quantity of acid sites per surface area of catalyst measured by NH₃-TPD decreases in the order of ZrO₂ > Zn_xZr_yO_z > ZnO. A slight shift in the overall NH₃ desorption toward lower temperatures with increasing Zn loading can be attributed to the stronger Lewis acidity of Zr⁴⁺ cations of m-ZrO₂ compared to t-ZrO₂.^{40–42} In fact, the relative strengths of the Lewis acid sites on ZrO₂ and Zn_xZr_yO_z catalysts can be compared by deconvoluting the NH₃-TPD spectra into weak and strong Lewis acid sites (NH₃ desorption peaks at 433 and 503 K). An example of this deconvolution is shown in Figure S4a, and the molar ratio of NH₃ desorption at stronger versus weaker Lewis acid sites is plotted as a function of Zn weight loading in Figure S4b. The quantities of weak and strong Lewis acid sites measured from this method are shown in Table S1. As the weight loading of Zn increases, the ratio of strong to weak Lewis acid sites decreases, consistent with the proposition that the addition of Zn passivates the strong Lewis acidity of ZrO₂. This trend continues up to a Zn weight loading of 8.0 wt % at which point the formation of bulk ZnO may prevent Zn from incorporating into the ZrO₂ lattice. We also note that, for bulk ZnO, the maximum NH₃ desorption occurs at approximately 504 K (Figure S5), suggesting that the Lewis acid sites, although significantly lower in concentration, are of moderate strength.

NH₃ desorption peaks at higher temperatures (greater than ~600 K) were not observed for any of the catalysts (see Figure S3a), further indicating that the concentration of Brønsted acid sites is insignificant. While no Brønsted acid sites were observed for these ex situ characterization techniques of the Zn_xZr_yO_z prepared via incipient wetness impregnation, it is possible that the dissociation of water under reaction conditions produces protons, which act as Brønsted acid sites, a subject discussed in Sections 3.3 and 3.4.

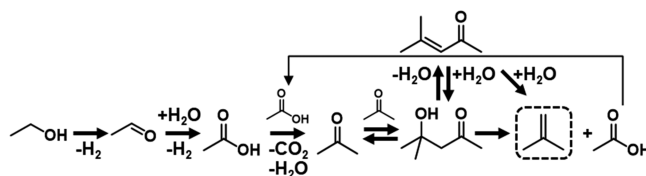
The Lewis basic sites on the catalyst surface were quantified by temperature-programmed desorption of CO₂. A representative CO₂-TPD plot is shown in Figure 1g over Zn_xZr_yO_z (2.2 wt % Zn), and the remainder of the plots are given in Figure S3b. A summary of the concentrations of Lewis basic sites is given in Table 1. Two peaks are observed in the CO₂-TPD

profile, a strong peak with a maximum CO₂ desorption around 375 K with a broad shoulder around 520 K and a small CO₂ desorption peak at around 865 K. Sun et al. have assigned the low-temperature peak to the desorption of weakly adsorbed CO₂ on the Lewis basic oxygen atoms of the hydroxyl groups on ZrO₂ and the high-temperature peak to CO₂ adsorbed on strong Lewis acid–base pairs (Zr⁴⁺–O²⁻).¹⁵ Consistent with the results of Sun et al., our CO₂-TPD results did not reveal a peak corresponding to weakly adsorbed CO₂ for ZnO, which only exhibits a single peak at approximately 700 K and not peaks at lower temperatures, which has been attributed to an absence of hydroxyl groups on the surface of ZnO.¹⁵

In summary, characterization of Zn_xZr_yO_z shows that this material consists of highly dispersed zinc oxide on the surface of tetragonal zirconia, with no evidence for ZnO nanoparticles. The surface of Zn_xZr_yO_z contains a balance between moderately Lewis acidic and basic sites. As shown in Figure 1c, varying the weight loading of Zn tunes the ratio of Lewis acidic to basic sites. This figure also shows that monoclinic ZrO₂ has a significantly higher Lewis acid to base ratio and that ZnO has a significantly lower Lewis acid to base ratio than Zn_xZr_yO_z. While the effects of Zn loading on the ratio of Lewis acidic to basic sites are subtle for Zn_xZr_yO_z, differences in this ratio can still be discerned. Evidence for these differences will be discussed in Sections 3.3 and 3.4 in the context of our studies of the reactions of ethanol and acetone to isobutene.

3.2. Proposed Reaction Pathway for Ethanol to Isobutene. In this section, we will propose a reaction pathway for the conversion of ethanol to isobutene. Evidence supporting this pathway and the site requirements for each step will be presented in Sections 3.3 and 3.4. The overall proposed reaction pathway for the conversion of ethanol to isobutene is shown by Scheme 1.

Scheme 1. Proposed Reaction Pathway for the Conversion of Ethanol to Isobutene



The first step in the proposed reaction pathway is the dehydrogenation of ethanol to produce acetaldehyde followed by oxidation to produce acetic acid. Two equivalent moles of acetic acid then undergo ketonization to produce one mole each of acetone, CO₂, and H₂O. Two moles of acetone then dimerize to produce diacetone alcohol, which undergoes decomposition to produce isobutene and acetic acid or, alternatively, undergoes reversible dehydration to produce mesityl oxide followed by hydrolysis to isobutene and acetic acid. The acetic acid produced in this last step undergoes further ketonization to produce more acetone, which then reacts further to produce isobutene.

Scheme 1 shows acetic acid, acetone, and mesityl oxide as reaction intermediates. The data shown in Table 2 present the Gibbs free energies of reaction for forming isobutene from ethanol, acetic acid, acetone, and mesityl oxide. The Gibbs free energies are calculated using density functional theory for a reaction temperature of 723 K. Also shown in this table are the maximum carbon selectivities for forming isobutene from each

Table 2. Reaction Stoichiometry and Free Energies of Formation for Ethanol, Acetic Acid, Acetone, and Mesityl Oxide Conversion to Isobutene

overall reaction	maximum theoretical carbon selectivity toward isobutene [%]	$\Delta G_{\text{rxn}, 723 \text{ K}}^a$ [kJ mol ⁻¹]
$3\text{EtOH} + \text{H}_2\text{O} \rightarrow 2\text{CO}_2 + 6\text{H}_2 + \text{C}_4\text{H}_8$	66.7	-235.9
$3\text{CH}_3\text{COOH} \rightarrow \text{C}_4\text{H}_8 + 2\text{CO}_2 + 2\text{H}_2\text{O}$	66.7	-228.1
$3\text{CH}_3\text{COCH}_3 \rightarrow 2\text{C}_4\text{H}_8 + \text{CO}_2 + \text{H}_2\text{O}$	88.9	-76.1
$3\text{C}_6\text{H}_{10}\text{O} + \text{H}_2\text{O} \rightarrow 4\text{C}_4\text{H}_8 + 2\text{CO}_2$	88.9	-266.0

^aGibbs free energies of formation calculated from DFT, with computational details provided in the Supporting Information.

starting compound. Computational details on the calculations are given in Figure S6.

The effect of space time, defined as the inverse of the weight-hourly space velocity (WHSV⁻¹), on the product distribution for the gas-phase conversion of ethanol to isobutene was investigated over Zn_xZr_yO_z (2.2 wt % Zn). These studies were conducted at 723 K with a steam-to-carbon (S/C) molar ratio of 5 as these reaction conditions showed the optimal selectivity towards isobutene. As the temperature increases, the rate of isobutene formation from acetone increases up to 723 K at which point the catalysts begin to deactivate. Isobutene selectivity also increases with increasing steam-to-carbon ratio, but the rate drops above S/C = 5 (see Figures S7 and S8). We note that at lower temperatures (698 K), higher selectivities toward desired products (4% isobutene, 10% acetaldehyde, and 53% acetone) can be attained for the

reaction of ethanol to isobutene (see Figure S9), which is high considering the theoretical carbon selectivity to acetone from ethanol is 75%. However, because the reaction rate is higher at 723 K, this temperature was selected for observation of reaction intermediates.

Figure 2a shows that as the space time increases, the conversion of ethanol over Zn_xZr_yO_z (2.2 wt % Zn) increases. At low space times, the principal products are acetaldehyde and acetone as well as CO₂. Smaller amounts of acetic acid and ethylene are also observed. As the space time increases, the selectivity to acetone reaches a maximum, whereas the selectivity to isobutene begins to rise monotonically, suggesting that acetone is an intermediate in the formation of isobutene. The selectivity to ethylene is invariant with space time, suggesting that this product is produced via a pathway that is not involved in the conversion of ethanol to isobutene, for example, by direct ethanol dehydration. Trace amounts of propene (pink, circle) are also observed and increase with increasing conversion of ethanol. The formation of propene likely comes from the dehydration of isopropanol, which is produced by reduction of acetone. We note that propene formation from ethanol over AgCeO₂/ZrO₂ and Y₂O₃-CeO₂ has been reported,^{43,44} and it has been proposed that the acetone is reduced to propanol by hydrogen transfer from ethanol via the Meerwein–Ponndorf–Verley (MPV) mechanism (see Scheme S1). The formation of methane, which is a result of acetone decomposition, also increases as space time increases.

Figure 2b shows the effect of space time on the product selectivity for the reaction of ethanol to isobutene over zinc oxide. The trends in the intermediates produced in the

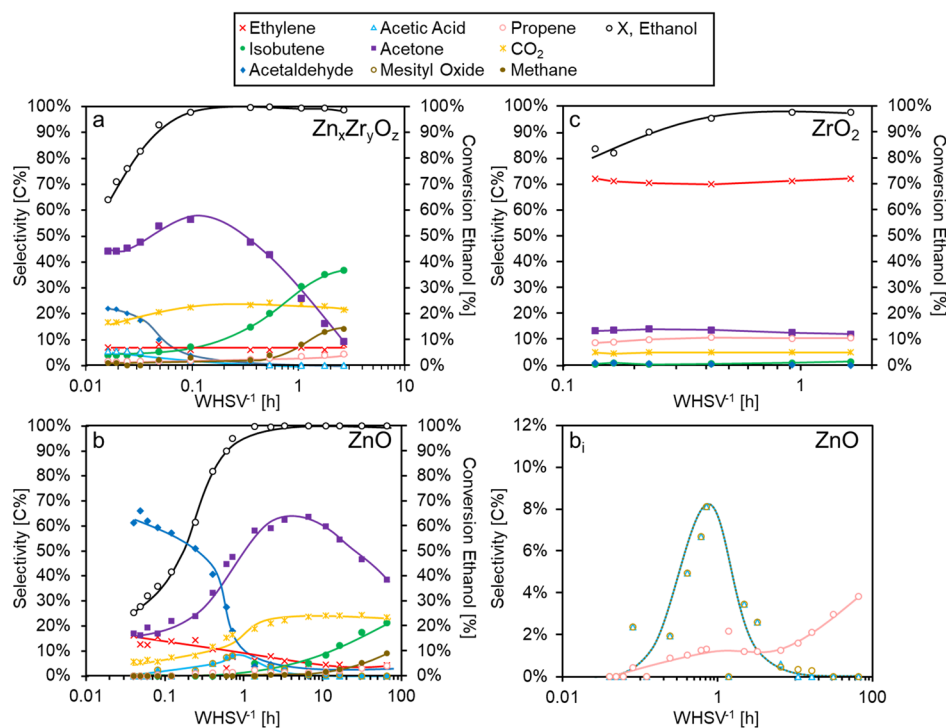


Figure 2. Effect of space time on ethanol conversion and product selectivity over (a) Zn_xZr_yO_z (2.2 wt % Zn), (b) bulk wurtzite ZnO, (b_i) bulk wurtzite ZnO (scale enlarged), and (c) monoclinic ZrO₂. Reaction conditions: 723 K, atmospheric pressure, 20–300 mL min⁻¹ He, (a) 4 mg of Zn_xZr_yO_z (2.2 wt % Zn), S/C 5, 0.16 kPa EtOH, 11.4 kPa H₂O, (b) 311 mg of ZnO, S/C = 5, 0.21 kPa EtOH, 11.4 kPa H₂O, (c) 22.4 mg of ZrO₂, S/C 2, 0.7 kPa EtOH, 30 kPa H₂O. WHSV is defined as the mass flow of reactants divided by the mass of catalyst (g h⁻¹ g⁻¹). Lines are a guide for the eye.

reaction are similar to those for $Zn_xZr_yO_z$ in Figure 2a; acetaldehyde and acetone are observed as intermediates, and the selectivity to isobutene, propene, and methane steadily increases with increasing space time. However, to achieve the same conversion of ethanol and product yields over ZnO as those over $Zn_xZr_yO_z$, an order of magnitude higher space time is required for ZnO. Other differences are observed, including a clear peak in the selectivity toward acetic acid and mesityl oxide at lower space times over ZnO compared to $Zn_xZr_yO_z$ (see Figure 2b_i).

Figure 2c shows that for the reaction of ethanol over ZrO_2 , the major product is ethylene, resulting from unimolecular dehydration of ethanol. Some acetone is formed, but only trace amounts of isobutene are produced and the selectivity to this product does not change significantly with increasing space time. The high selectivity to ethylene over ZrO_2 even in the presence of water is not surprising as zirconia is known to catalyze the unimolecular dehydration of alcohols.^{45,46} Because of the subtler differences in the reaction intermediates observed over $Zn_xZr_yO_z$ (2.2 wt % Zn) compared to ZnO, we will place more of a focus on comparing reactions over these two catalysts in subsequent sections.

3.3. Ethanol Conversion to Acetone. In this section, we focus on the steps involved in the conversion of ethanol to acetone, a critical intermediate in producing isobutene. We use a combination of experimental evidence and information taken from the literature to propose a mechanism for each of the following steps: ethanol dehydrogenation to acetaldehyde, acetaldehyde oxidation to acetic acid, and ketonization of acetic acid to acetone, and to propose what types of sites are required for each step. The elementary processes involved in the conversion of acetone to isobutene are discussed in Section 3.4.

3.3.1. Ethanol Dehydrogenation to Acetaldehyde. The proposed first step in the reaction of ethanol to isobutene is the dehydrogenation of ethanol to acetaldehyde and H_2 . The observation of a maximum in the rate of acetaldehyde production over $Zn_xZr_yO_z$ (2.2 wt % Zn) at low ethanol conversions, seen in Figure 2a, suggests that acetaldehyde is an intermediate in the reaction pathway. Additional information on the role of the acid–base properties of the catalyst in the dehydrogenation of ethanol to acetaldehyde and the competing reaction, ethanol dehydration, was obtained by measuring the ethanol conversion and product selectivities for ZrO_2 , $Zn_xZr_yO_z$, and ZnO at 698 K, as shown in Figure 3.

Acetaldehyde is observed for all the $Zn_xZr_yO_z$ catalysts as well as bulk ZnO, as shown in Figure 3a. Some acetaldehyde can also be observed for the reaction of ethanol over ZrO_2 although the selectivity to this product is minimal. Because the basicity and acidity of the catalysts change with weight loading of Zn, the ethanol conversion and the product selectivities can be correlated with the ratio of Lewis acidity to basicity quantified by NH_3 -TPD and CO_2 -TPD, respectively. As shown in Figure 3b, the conversion of ethanol decreases as the ratio of Lewis acidity to basicity increases. The addition of Zn to zirconia greatly suppresses ethanol dehydration by passivating the Lewis acidity and introducing basicity, as evidenced by the minimum in ethylene selectivity for the catalysts with intermediate ratios of acid to base sites (red line and square points). However, the ethylene selectivity increases slightly over ZnO, possibly as a result of strong base-catalyzed dehydration. The selectivity to acetone is also highest for $Zn_xZr_yO_z$ containing 2.2 wt % Zn. There is a clear relationship

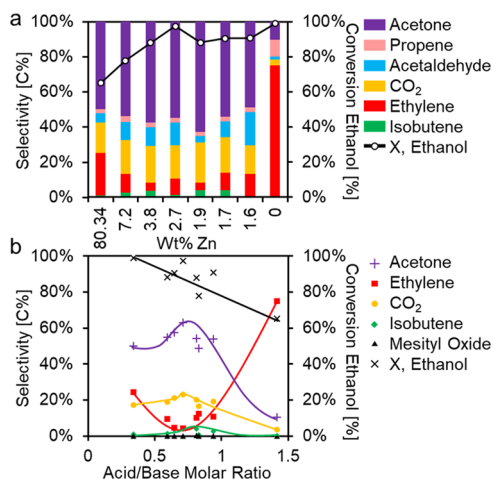


Figure 3. (a) Conversion and selectivity of ethanol conversion over ZnO, ZrO_2 , and $Zn_xZr_yO_z$ as a function of Zn loading and (b) selectivity as a function of acid/base molar ratio. Reaction conditions: 698 K, 1 kPa EtOH, S/C = 4, 50 mL min^{-1} He, 1 m^2 catalyst.

between the rate of ethanol consumption and basicity (Figure S10b) but not acidity (Figure S10a), further supporting the idea that ethanol dehydrogenation to acetaldehyde is base-catalyzed. From the relationship between the Lewis acid/base ratio and the reaction selectivity, it is clear that minimizing ethylene production requires an optimal ratio of Lewis acid to base sites, which can be achieved with $Zn_xZr_yO_z$. We also found that ethanol dehydration increases in the absence of water over $Zn_xZr_yO_z$, as shown in Figure 4 and Figure S11.

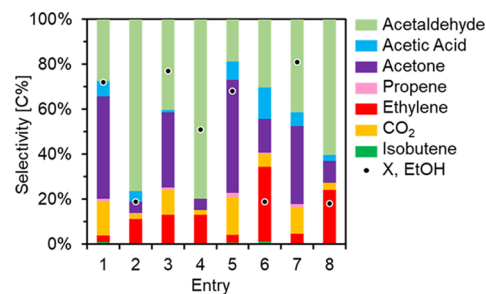


Figure 4. Reactions of ethanol and acetaldehyde over ZnO and $Zn_xZr_yO_z$. Reaction conditions given in Table 3. For carbon selectivity calculations, acetaldehyde is considered a product, despite being cofed in entries 5–8.

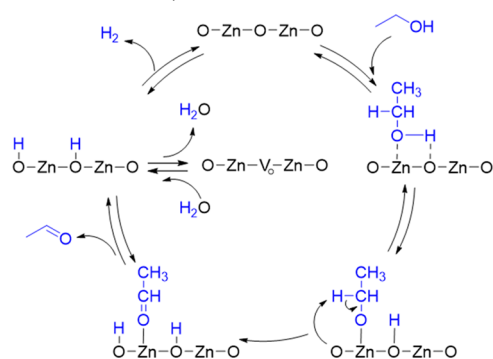
The combination of strong Lewis basicity introduced by dispersing Zn on the catalyst surface and the inhibition of dehydration by water is therefore expected to be responsible for promoting ethanol dehydrogenation over $Zn_xZr_yO_z$ and ZnO.

Prior studies have shown that ethanol dehydrogenation is Lewis base-catalyzed and inhibited by water,^{47,48} whereas the ethanol dehydration is catalyzed by Brønsted or Lewis acidity,^{49–52} and inhibited by water.^{49,50} Of particular note for the present study, Vohs and Barteau have suggested that over the (0001)-Zn surface of ZnO, ethanol and 1-propanol dehydration and dehydrogenation share a common intermediate, an ethoxide, formed by dissociative adsorption of ethanol onto the catalyst surface.⁵³

Based upon our experimental results and proposed mechanisms for ethanol dehydrogenation in the literature,

we propose a mechanism for the Lewis acid–base-catalyzed dehydrogenation of ethanol to produce acetaldehyde over the zinc–zirconia mixed oxide catalysts, shown in Scheme 2.

Scheme 2. Proposed Mechanism for the Dehydrogenation of Ethanol over $Zn_xZr_yO_z$



Although the surface contains Zn–O–Zr moieties, the surface is drawn as ZnO for simplicity because it is estimated that the surface coverage of ZnO exceeds one monolayer for the mixed oxide catalysts. The first step is the dissociative adsorption of ethanol over a Lewis acid Zn^{2+} site on the catalyst surface to produce a bound alkoxide. This is followed by the rate-limiting Lewis base-catalyzed abstraction of an α -hydrogen, breaking a C–H bond and forming a C=O bond. The final step is the desorption of acetaldehyde. The hydrogen can then leave as H_2 or as water via the Mars–van Krevelen (MVK) mechanism, leaving an oxygen vacancy on the surface. This vacancy is replenished by water, which dissociates on the surface. While acetaldehyde is observed as a product at low space times, it is not observed at high space times, that is, high ethanol conversions, suggesting that as the concentration of acetaldehyde starts to build up, its conversion to acetic acid is accelerated.

3.3.2. Oxidation of Acetaldehyde to Acetic Acid. The next step in the proposed reaction pathway for the formation of isobutene from ethanol is oxidation of acetaldehyde (or an adsorbed alkoxide) to produce acetic acid (or a surface acetate species). Acetic acid is observed as an intermediate at low space times over ZnO (Figure 2b_i) but is not observed for the reaction of ethanol over $Zn_xZr_yO_z$ (Figure 2a). This is likely due to the rapid ketonization of acetic acid to produce acetone over $Zn_xZr_yO_z$, as discussed further in Section 3.3.3.

To deduce the reaction pathway for the oxidation of acetaldehyde to acetic acid over $Zn_xZr_yO_z$, we compared the reaction of ethanol and mixtures of ethanol and acetaldehyde over $Zn_xZr_yO_z$ and ZnO in the presence and absence of water. Mixtures of ethanol and acetaldehyde (50 wt %) were used to ensure that the reactants were introduced in the liquid phase before vaporizing in the feed line to the reactor. Figure 4 gives key results for these reactions, and the reaction conditions for each experiment are given in Table 3.

Water is necessary to promote the reactions of ethanol and ethanol/acetaldehyde mixtures over both $Zn_xZr_yO_z$ and ZnO, as evidenced by the significantly lower conversions observed in the absence of water (entries 2, 4, 6, and 8) compared to those attained in the presence of water (entries 1, 3, 5, and 7). The conversions shown in entries 2, 4, 6, and 8 correspond to initial conversion and selectivity, because both $Zn_xZr_yO_z$ and ZnO rapidly deactivate in the absence of water (see Figure S12a,b).

Table 3. Reaction Conditions for Figure 4^a

entry	feedstock	catalyst	catalyst mass [mg]	feedstock partial pressure [kPa]	partial pressure H_2O [kPa]
1	ethanol	$Zn_xZr_yO_z$ 2.2 wt % Zn	4.8	0.16	13
2	ethanol	$Zn_xZr_yO_z$ 2.2 wt % Zn	4.8	0.16	0
3	ethanol	ZnO	58	0.19	13
4	ethanol	ZnO	58	0.19	0
5	ethanol/ acetaldehyde	$Zn_xZr_yO_z$ 2.2 wt % Zn	4.8	0.14	13
6	ethanol/ acetaldehyde	$Zn_xZr_yO_z$ 2.2 wt % Zn	4.8	0.14	0
7	ethanol/ acetaldehyde	ZnO	60.1	0.13	13
8	ethanol/ acetaldehyde	ZnO	60.1	0.13	0

^aAdditional reaction conditions for entries 1–8: 723 K, 150 mL min^{-1} He, atmospheric pressure.

As discussed in Section 3.3.1, the ethanol selectivity to ethylene is higher over ZnO than (2.2 wt % Zn) in the presence of water, as shown by entries 1 and 3 in Figure 4. Over $Zn_xZr_yO_z$, the selectivity to ethylene is relatively unchanged when acetaldehyde is co-fed with ethanol in the presence of water (entry 5 compared to entry 1). However, over ZnO, the selectivity to ethylene is lower when acetaldehyde is co-fed (entry 7 compared to entry 3).

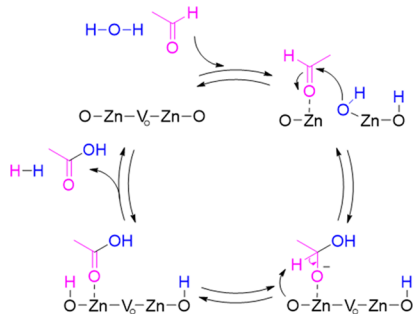
The selectivity to acetic acid is generally higher when acetaldehyde is co-fed with ethanol (entries 5–8), suggesting that acetaldehyde is an intermediate in acetic acid formation. Slightly higher amounts of acetic acid are observed over $Zn_xZr_yO_z$ (entries 1, 2, 5, 6) compared to ZnO (entries 3, 4, 7, 8), suggesting that the oxidation of acetaldehyde is promoted by balanced acid/base sites present on the surface of $Zn_xZr_yO_z$. Ethyl acetate was not observed for any of the reactions, suggesting that the oxidation of acetaldehyde over $Zn_xZr_yO_z$ and ZnO occurs via hydroxyl addition to acetaldehyde as opposed to the decomposition of ethyl acetate, as proposed for the formation of acetone from ethanol over $Y_2O_3-CeO_2$.⁴⁴

It has been proposed that acetaldehyde oxidation to acetic acid occurs via direct participation of surface hydroxyl groups from adsorbed water over Sc/In_2O_3 ⁴⁴ and $ZnO-CaO$.⁵⁴ Rahman et al. found that water inhibits the aldolization of acetaldehyde to crotonaldehyde over ZnO, favoring instead the oxidation of acetaldehyde to acetic acid, which undergoes ketonization to produce acetone.⁵⁵ Silva-Calpa et al. have shown that the addition of Zn to monoclinic zirconia produces defect sites in the form of oxygen vacancies that improve the redox properties of the catalyst and promote the dissociation of water on the surface.⁵⁶ In a subsequent study of the conversion of ethanol to acetone over $Zn_xZr_{1-x}O_{2-y}$, the authors suggested that acetaldehyde reacts with the oxygen of the solid solution to produce vacancies on the catalyst surface and then undergoes ketonization to acetone and CO_2 followed by the dissociation of water over vacancy sites to re-oxidize the surface.⁵⁷ The formation of oxygen vacancies by the addition of Zn and Zr dopants to metal oxides has been shown to improve the mobility of lattice oxygen participating in the Mars–van Krevelen mechanism, in addition to modifying the

acid–base properties.^{58,59} Other studies have shown that oxygen vacancies are able to promote the dissociation of water to produce surface hydroxyl groups over ceria⁶⁰ and zirconia.⁶¹ Moreover, theoretical investigations of the partial dissociation of H₂O over ZnO (1011) have concluded that the hydrogen bonding of water aids in water dissociation; therefore, the greater the surface coverage of water, the greater the water dissociation.⁶²

Our experimental evidence indicating that water is critical for the oxidation of acetaldehyde and that balanced Lewis acid/base sites promote the oxidation of acetaldehyde, together with evidence for the role of water dissociation in the oxidation of acetaldehyde given in the literature,^{44,54–57,59–62} lead us to propose the mechanism for the oxidation of acetaldehyde to acetic acid shown in Scheme 3.

Scheme 3. Proposed Mechanism for the Oxidation of Acetaldehyde over Zn_xZr_yO_z



Acetaldehyde first adsorbs onto a Lewis acid site, and water dissociates onto the catalyst surface over oxygen vacancies. These steps are followed by the addition of a hydroxyl group to the carbonyl carbon atom and then base-catalyzed hydrogen abstraction and formation of the carbon–oxygen double bond to produce bound acetic acid. The acetic acid can either desorb or remain on the surface to undergo ketonization in the next step.

3.3.3. Ketonization of Acetic Acid to Acetone. The next step in the proposed reaction pathway is ketonization of acetic acid to produce acetone. As shown earlier in Figure 2b, at low space times, the reaction of ethanol over ZnO yields a small amount of acetic acid, which is generated and then consumed as the space time increases. In contrast, as shown in Figure 2a, no significant amounts of acetic acid can be observed for the reaction of ethanol over Zn_xZr_yO_z (2.2 wt % Zn). This suggests that acetic acid reacts more rapidly over Zn_xZr_yO_z than over ZnO, indicating that ketonization requires a higher concentration of Lewis acid sites. To further probe the reactivity of acetic acid, we studied the reaction of acetic acid over ZnO and Zn_xZr_yO_z (2.2 wt % Zn) in the presence and absence of water.

The reaction of acetic acid to produce isobutene over Zn_xZr_yO_z (2.2 wt % Zn) is stable for over 5 h at 723 K for a steam-to-carbon ratio of 5.4, as shown in Figure S13. Interestingly, in contrast to the literature,¹⁹ we found that bulk ZnO is also capable of catalyzing the ketonization of acetic acid to acetone and subsequent isobutene formation at 723 K and remains stable even though the reaction is much slower than over Zn_xZr_yO_z. The two leftmost entries in Figure 5 show a comparison of Zn_xZr_yO_z (2.2 wt % Zn) and bulk ZnO for the reaction of acetic acid in the presence of water at 723 K under the same reaction conditions and using the same

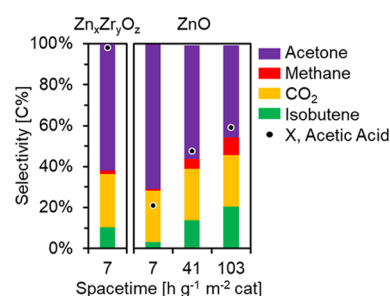


Figure 5. Reaction conditions: left: 22.3 mg of Zn_xZr_yO_z (2.2 wt % Zn), 723 K, 0.16 kPa acetic acid, 11.4 kPa H₂O, S/C = 5.4; right: 319 mg of ZnO, 723 K, 0.18 kPa acetic acid, 13 kPa H₂O, S/C = 5.7.

catalyst surface area. The conversion of acetic acid is greater over the mixed oxide catalyst, and the rate of isobutene formation is over 3 times greater over the Zn_xZr_yO_z compared to ZnO (4.11×10^{-5} mol h⁻¹ m⁻² versus 1.25×10^{-5} mol h⁻¹ m⁻², respectively). As shown in the three rightmost entries of Figure 5, the selectivity to isobutene can be increased over ZnO as the space time and hence the conversion of acetic acid increase. To reach the same rate of isobutene formation over ZnO as that observed over the mixed oxide catalyst, the space time needs to be increased by approximately a factor of 4. Still, the reaction pathway and intermediates appear to be the same over ZnO as they are over Zn_xZr_yO_z although as the conversion is increased, the selectivity to methane over ZnO also increases.

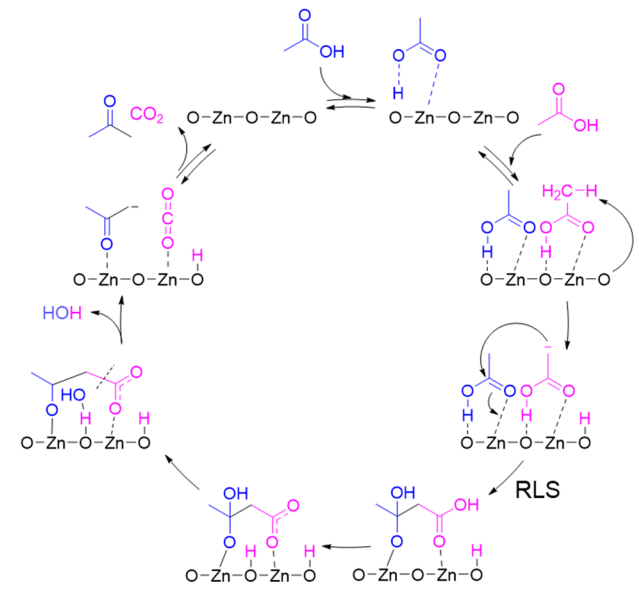
In the absence of water, the rate of acetic acid consumption over both ZnO and Zn_xZr_yO_z decreases rapidly due to catalyst deactivation. As shown in Figure S14a,b, the initial rate of isobutene formation is high, but the catalyst deactivates immediately and produces significant amounts of acetic anhydride, as well as small amounts of methane. This suggests that water, while inhibiting active sites for acetic acid adsorption, inhibits undesired acetone decomposition to methane and bimolecular dehydration of acetic acid to produce acetic anhydride. Furthermore, at a constant steam-to-carbon ratio, there is an increase in the rate of isobutene formation and selectivity with increasing acetic acid partial pressure (see Figure S15), suggesting that the surface is not saturated with acetic acid. The clear differences in the reaction rates of acetic acid over ZnO and Zn_xZr_yO_z suggest that the balanced acid–base pairs on Zn_xZr_yO_z are more effective for the ketonization step than the strong Lewis basic sites on bulk ZnO.

Previous studies have suggested that Lewis acid–base pairs promote ketonization of acetic acid over Zn_xZr_yO_z prepared via sol–gel synthesis¹⁹ and that the acid–base properties of the catalyst or coordination vacancies play a critical role in catalyzing the ketonization reaction over metal oxides.⁶³ Wang and Iglesia have suggested that the rate-limiting step for ketonization of C₂–C₄ carboxylic acids over TiO₂ and ZrO₂ is C–C bond formation between 1-hydroxy enolate species and co-adsorbed acids bound at neighboring acid–base pairs saturated with active monodentate carboxylates.⁶⁴ Gumidyala et al. also proposed that C–C coupling is the rate-limiting step for acid-catalyzed ketonization of acetic acid over H-ZSMS and that water inhibits the reaction rate but improves catalyst stability.⁶⁵ Gangadharan et al. have suggested that water promotes propanal ketonization and inhibits aldol condensation over ceria modified zirconia (Ce_xZr_{1-x}O₂) by increasing the concentration of surface –OH groups that enhance the

formation of surface carboxylates with the aldehyde.⁶⁶ A DFT study of acetic acid ketonization over tetragonal zirconia reported by Tosoni et al. has also highlighted the beneficial role of oxygen vacancies and reduced Zr^{3+} centers for the ketonization reaction. The authors propose that the reaction proceeds via adsorption of acetic acid followed by formation of an enolate and an acyclic intermediate, which react together to form the β -keto acid.⁶⁷

Based upon our experimental observations and the precedent for Lewis acid–base-catalyzed ketonization in the literature, we propose the mechanism for ketonization of acetic acid to produce acetone and CO_2 over $Zn_xZr_yO_z$ shown in Scheme 4. First, two acetic acid molecules adsorb onto acid–

Scheme 4. Proposed Mechanism for the Ketonization of Acetic Acid over $Zn_xZr_yO_z$.



base pairs, with the basic oxygen interacting with the hydrogen on the hydroxyl group and the Lewis acidic Zn^{2+} interacting with the carbonyl oxygen. Next, a basic oxygen abstracts a hydrogen from the methyl group, producing a carbanion, which then attacks the carbonyl group of the second acetic acid to form a C–C bond in the rate-limiting step to produce an adsorbed dimer. From there, subsequent dehydration and C–C bond cleavage produce CO_2 and acetone. The importance of Lewis acidity is clear in the rate-limiting step as the Zn^{2+} cation must be sufficiently acidic to activate the adsorbed acetic acid. We also point out that acetic acid ketonization is typically carried out at lower temperatures (~ 503 to 603 K)^{64,65} as opposed to 723 K, further suggesting that water is necessary to prevent side reactions that may occur more readily at higher temperatures. Desorption of acetone in the final step is reversible, because although significant amounts of acetone are observed for this reaction, the dimerization of acetone requires the adsorption of acetone on the catalyst surface.

3.4. Conversion of Acetone to Isobutene. As demonstrated in Section 3.3, acetone is a critical intermediate in the cascade of reactions leading from ethanol to isobutene. The mechanism for the conversion of acetone to isobutene is difficult to probe as intermediates such as diacetone alcohol are unstable, and it is unclear whether mesityl oxide is an intermediate in this reaction pathway and what role water plays

in promoting the decomposition of C_6 intermediates to isobutene and acetic acid. In this section, we discuss the condensation of acetone to diacetone alcohol and investigate the role of mesityl oxide in the conversion of acetone to isobutene. We then propose a reaction mechanism and use it to develop a rate expression for the conversion of acetone to isobutene.

3.4.1. Acetone Condensation to Diacetone Alcohol. The first step in the proposed reaction pathway for the conversion of acetone to isobutene is the dimerization of acetone to produce diacetone alcohol. The product distribution observed upon feeding diacetone alcohol to the reactor is nearly identical to that observed when acetone is the feed. In fact, upon introduction into the reactor via a syringe pump through heated lines (~ 367 K), the diacetone alcohol is already completely converted to acetone before reaching the catalyst bed, suggesting that this reaction step is reversible and that equilibrium lies strongly to the left. This finding is consistent with the calculated gas-phase free energy of reaction ($+110.8$ kJ mol⁻¹), which indicates that the reaction of acetone to diacetone alcohol is strongly disfavored (Figure S6). Studies in the literature indicate that both Brønsted acid sites and Lewis acid–base pairs can facilitate the activation of acetone.^{68–71} Therefore, we assume that Lewis acid–base sites on the surface of $Zn_xZr_yO_z$ are responsible for promoting the dimerization of acetone to diacetone alcohol.

3.4.2. Reaction of Mesityl Oxide to Isobutene. Mesityl oxide is observed as a secondary product at low conversions for the reaction of ethanol to isobutene over bulk ZnO , and at low conversions for the reaction of acetone to isobutene over both ZnO and $Zn_xZr_yO_z$ (2.2 wt % Zn) (see Figure 2b_i and Figure S7). However, the role of mesityl oxide as an intermediate is unclear. To better understand the role of mesityl oxide in the conversion of acetone to isobutene, the reaction of mesityl oxide to isobutene was investigated over both $Zn_xZr_yO_z$ (2.2 wt % Zn) and ZnO .

Figure 6 shows the product distribution for reactions of mesityl oxide (90%, remainder 4-methylpent-4-en-2-one) over

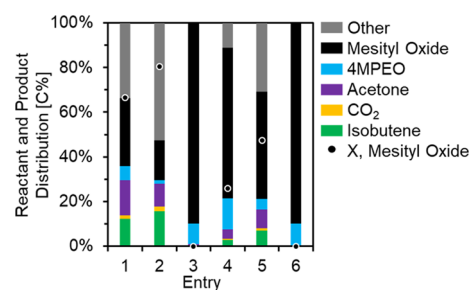


Figure 6. Product distribution for the reaction of mesityl oxide over $Zn_xZr_yO_z$ (2.2 wt % Zn) and ZnO at varying space times and in the presence and absence of water. Reaction conditions are given in Table 4.

$Zn_xZr_yO_z$ (2.2 wt % Zn) and ZnO at two different space times (Table 4, entries 1 and 2 and 4 and 5, respectively) and in the absence of water (Table 4, entries 3 and 6). As shown in Figure 6 and Table 4, entries 1 and 2 and 5 and 6, both isobutene and acetone are formed. This indicates that the acetone-to-diacetone alcohol-to-mesityl oxide pathway is reversible under reaction conditions. Therefore, it is not clear whether the reaction to form isobutene proceeds via hydrolysis of mesityl oxide or whether the mesityl oxide is only a side

Table 4. Reaction Conditions for Figure 6^a

entry	catalyst	catalyst mass [mg]	space time [hr g cat ⁻¹ m ⁻²]	partial pressure H ₂ O [kPa]
1	Zn _x Zr _y O _z 2.2 wt % Zn	4.9	1.7	13
2	Zn _x Zr _y O _z 2.2 wt % Zn	4.9	21.8	13
3	Zn _x Zr _y O _z 2.2 wt % Zn	4.9	1.7	0
4	ZnO	60.8	1.5	13
5	ZnO	60.8	17.8	13
6	ZnO	60.8	1.5	0

^aAdditional reaction conditions: 723 K, 0.012 kPa initial 4-methylpent-4-en-2-one, 0.12 kPa initial mesityl oxide, 150 mL min⁻¹ He (entries 1, 3, 4, 6), 11.8 mL min⁻¹ He (entry 2), 12.4 mL min⁻¹ He (entry 5). Entries 1,2,4,5, S/C = 6.3. Entries 3 and 6, taken after 15 min time on stream.

product. Increasing the space time for the reaction of mesityl oxide and water over Zn_xZr_yO_z (Table 4, entries 1 and 2) and ZnO (Table 4, entries 4 and 5) increases the selectivity to isobutene and the conversion of mesityl oxide and decreases the selectivity to acetone, suggesting that acetone may be an intermediate in the formation of isobutene from mesityl oxide and water. As the space time increases, there is an increase in the formation of other side products, such as isophorone and higher C₉₊ compounds, resulting from the condensation of mesityl oxide with acetone. These products are not observed for the reaction of acetone and water over these catalysts under the same reaction conditions and steam-to-carbon ratios, suggesting that mesityl oxide is an intermediate for the formation of side products. In contrast to the reaction of acetone to isobutene, for the reaction of mesityl oxide, both Zn_xZr_yO_z and ZnO deactivate over the course of a few hours, even in the presence of water, as shown in Figure S16a,b. In the absence of water, the activity of the catalysts decreases rapidly after approximately 15 min of time on stream, as shown by entries 3 and 6 in Table 4. Evidence for coke formation was observed by the formation of high carbon number products (C₉₊) as well as visual observation of black deposits on the catalyst after the reaction.

The initial feed for the mesityl oxide experiments contains an equilibrated mixture of mesityl oxide with 10 mol % of the isomer 4-methylpent-4-en-2-one (4MPEO). At low space times for the reaction of mesityl oxide over Zn_xZr_yO_z and ZnO in the presence of water, the percentage of 4MPEO relative to mesityl oxide increases to 17 mol % (entries 1 and 4). At higher space times, however, the percentage of 4MPEO drops to 8 and 9 mol % over Zn_xZr_yO_z and ZnO, respectively. In the absence of water, the activity of both catalysts is almost negligible, and the relative percent of 4MPEO is close to that in the feed (9 and 10 mol % 4MPEO for Zn_xZr_yO_z and ZnO, respectively). The increase in the relative partial pressure of 4MPEO at low space times suggests that mesityl oxide may undergo isomerization or that mesityl oxide is consumed more rapidly than 4MPEO.

From these data, we conclude that over Zn_xZr_yO_z and ZnO, the conversion of two molecules of acetone to produce mesityl oxide and water is reversible under reaction conditions, that increasing space time leads to increasing conversion of mesityl oxide, and that the mechanism of catalyst deactivation comes from the formation of condensation products that further oligomerize and contribute to coke formation. Because of the reversible nature of the acetone to mesityl oxide reaction, it

remains unclear at this stage whether mesityl oxide is a necessary intermediate for the formation of isobutene. To further probe the acetone to isobutene reaction, additional rate measurements and isotopic labeling experiments were performed.

3.4.3. Kinetic Isotope Effects for the Reaction of Acetone to Isobutene. The kinetic isotope effect for the reaction of acetone to isobutene was measured for both Zn_xZr_yO_z and ZnO to identify the rate-limiting step. A reaction temperature of 623 K was selected so that rates of both mesityl oxide and isobutene formation could be measured at low conversions and with negligible catalyst deactivation. The results of the kinetic isotope effect measurements are shown in Table 5. In

Table 5. Kinetic Isotope Effect Experiments for Acetone Conversion to Isobutene and Mesityl Oxide^a

reactants	observed KIE isobutene (k_H/k_D)		observed KIE mesityl oxide (k_H/k_D)	
	Zn _x Zr _y O _z (2.2 wt % Zn)	ZnO	Zn _x Zr _y O _z (2.2 wt % Zn)	ZnO
acetone- <i>d</i> ₆ and D ₂ O	0.96 ± 0.20	1.34 ± 0.10	1.11 ± 0.10	1.11 ± 0.10
acetone- <i>d</i> ₆ and H ₂ O	1.02 ± 0.29	1.12 ± 0.11	1.20 ± 0.11	1.07 ± 0.10
acetone and D ₂ O	1.01 ± 0.10	1.14 ± 0.10	1.08 ± 0.10	1.18 ± 0.10

^aReaction conditions: 623 K, 1 kPa acetone/acetone-*d*₆, 15 kPa H₂O/D₂O, WHSV 2.2 h⁻¹, 50 mL min⁻¹ He, 1 atm.

agreement with Sun et al., we did not observe a significant kinetic isotope effect for the formation of isobutene from acetone over Zn_xZr_yO_z.¹⁶ We also measured kinetic isotope effects for the formation of isobutene from acetone over ZnO and did not observe a kinetic isotope effect. These findings indicate that C–H bond cleavage is not involved in the rate-limiting step for the reaction of acetone to isobutene over either Zn_xZr_yO_z or ZnO and suggest that the rate-limiting step for isobutene formation is not the dehydration of diacetone alcohol to produce mesityl oxide. We propose, instead, that it must be either C–C bond formation occurring during acetone coupling to form diacetone alcohol or the decomposition of diacetone alcohol, which does not involve the breaking of C–H or O–H bonds. The formation of mesityl oxide was also not significantly affected by deuteration of either acetone or water over either Zn_xZr_yO_z or ZnO, confirming that unimolecular dehydration of diacetone alcohol is not rate-limiting for the dominant pathway toward forming either mesityl oxide or isobutene.

The slight kinetic isotope effect for isobutene formation over ZnO in the presence of acetone-*d*₆ and D₂O and for mesityl oxide formation in the presence of acetone-*d*₆ may be due to minor pathways toward isobutene and mesityl oxide formation that are limited by activation of water or C–H bond cleavage; however, because these kinetic isotope effects are small and nearly within error, we suggest that the rate-limiting step for the dominant pathway for isobutene formation is either C–C coupling or decomposition of diacetone alcohol and that C–C coupling is the rate-limiting step for the dominant pathway for mesityl oxide formation.

3.4.4. Roles of Acidity and Basicity for the Conversion of Acetone to Isobutene. The kinetic isotope experiments do not reveal whether the mechanism of acetone conversion to

isobutene is different over $Zn_xZr_yO_z$ versus ZnO . To further investigate the nature of the active sites for this reaction, the effect of Lewis acidity and basicity on the selectivity for the reaction of acetone to isobutene was probed. As demonstrated previously, the acid–base properties of $Zn_xZr_yO_z$ can be tuned by adjusting the weight loading of Zn on the surface. The effect of Zn loading on the selectivity and activity for the acetone to isobutene reaction is shown in Figure 7a in which 0 wt % Zn corresponds to pure monoclinic zirconia and 80.3 wt % Zn corresponds to bulk zinc oxide.

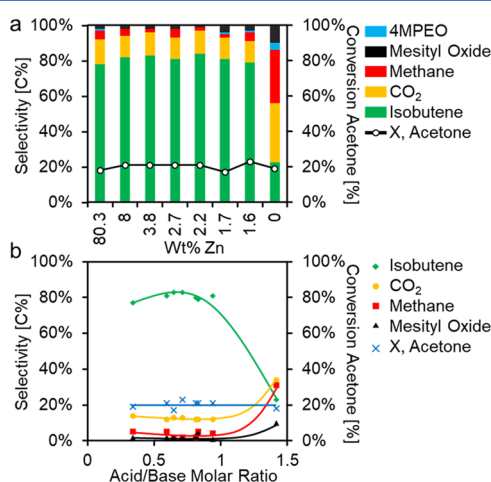


Figure 7. (a) Conversion of acetone to isobutene as a function of Zn weight loading. (b) Conversion and selectivity for the acetone to isobutene reaction as a function of acid/base ratio. Reaction conditions: 698 K, 0.5 kPa acetone, 30 kPa H_2O , S/C = 8.2, 50 $mL\ min^{-1}$ He, 1 m^2 catalyst.

Interestingly, above a Zn loading of 1.6 wt %, the selectivity to isobutene remains relatively unchanged, exhibiting nearly theoretical isobutene selectivities ($\sim 80\%$), with some minor formation of methane and trace amounts of mesityl oxide. In contrast to the reaction of ethanol to isobutene, no propene was observed, further suggesting that alcohols are required in the feed to serve as reducing agents for the MPV reduction of acetone to isopropanol, which then dehydrates to form propene. The conversions for these catalysts are nearly the same despite the differences in acidity and basicity. To assess the effects of catalyst acid–base properties on the selectivity of the acetone to isobutene reaction, the conversion and selectivity toward isobutene, methane, and mesityl oxide were plotted versus the total basicity measured from CO_2 -TPD, the total acidity measured via NH_3 -TPD, and the ratio of Lewis acid to base concentrations. These plots are shown in Figure S17a,b and Figure 7b, respectively. Figure 7b clearly shows that the most acidic catalyst (ZrO_2) exhibits higher methane formation. This is in agreement with the results of Takanabe et al., who found that CO_2 and CH_4 were the major products of steam reforming of acetone over ZrO_2 .⁷² Therefore, we suggest that the addition of Zn suppresses the decomposition of acetone to methane by lowering both the strength and quantity of Lewis acid sites.

Apart from the highly acidic ZrO_2 , which exhibits a lower isobutene selectivity, there is no clear correlation between catalyst acidity and basicity, and the observed trends in product selectivity (Figure S17a,b). However, by plotting product selectivity versus the molar ratio of acid to base sites

for each of the catalysts tested (Figure 7b), the subtler effects of Lewis acid/base ratios on selectivity can be observed for $Zn_xZr_yO_z$. The 2.2 wt % Zn catalyst exhibits a slightly higher isobutene selectivity and the lowest selectivity toward side products (methane, mesityl oxide, etc.) compared to catalysts with other weight loadings of Zn. This catalyst has an acid/base molar ratio of approximately 0.71. XRD and Raman spectroscopy show that, at a Zn weight loading of 2.2%, nearly all the zirconia has transformed from the monoclinic to the tetragonal phase (Figure 1a,b), suggesting that the surface contains a sufficient coverage of Zn to stabilize the tetragonal phase but does not yet form bulk ZnO clusters. As mentioned in Section 3.1, this suggests that the Zn–O–Zr interactions are more predominant at this intermediate Zn weight loading and that these moieties are beneficial for promoting the reaction of acetone to isobutene. We therefore conclude that the formation of isobutene from acetone requires a balance of Lewis acid and base sites.

3.4.5. Kinetics of the Acetone to Isobutene Reaction. To gain further insight into the mechanism and kinetics of acetone conversion to isobutene, a series of experiments were performed under conditions of differential conversion ($<7\%$) in which the effects of temperature, water partial pressure, and acetone partial pressure on the rates of formation of isobutene and mesityl oxide were measured.

Figure 8 shows the effects of water and acetone partial pressure on the rates of isobutene and mesityl oxide formation

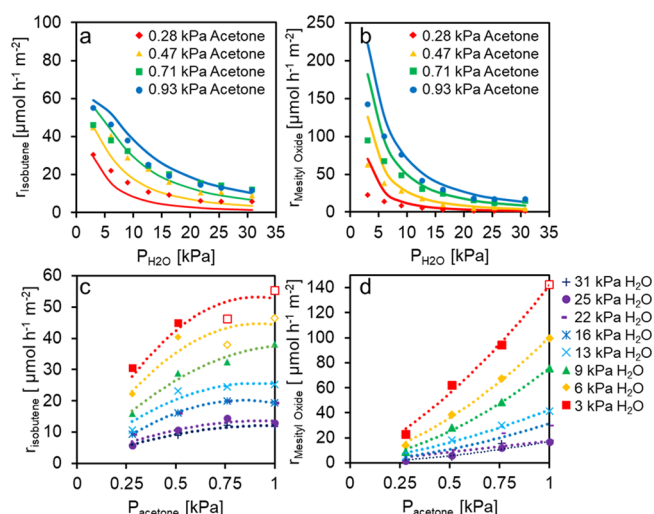


Figure 8. (a) Effect of water partial pressure on the rate of isobutene formation, (b) effect of water partial pressure on the rate of mesityl oxide formation, (c) effect of acetone partial pressure on the rate of isobutene formation, (d) effect of acetone partial pressure on the rate of mesityl oxide formation. Reaction conditions: 623 K, atmospheric pressure, 5.5 mg of $Zn_xZr_yO_z$ (2.2 wt % Zn), 50 $mL\ min^{-1}$ He. Solid lines represent a fit to the kinetic model given by eq 2. Dashed lines are a guide for the eye. Hollow data points refer to initial rates after which the catalyst rapidly deactivates.

over $Zn_xZr_yO_z$ (2.2 wt % Zn) at 623 K. As evidenced by Figures 8a,b, water inhibits both isobutene and mesityl oxide formation; however, water is necessary to prevent deactivation, which occurs when the steam-to-carbon ratio drops below 5. Figure 8c,d shows that the rate of isobutene formation lies between zero and first order in acetone partial pressure and the rate of mesityl oxide formation is between first and second order in acetone partial pressure. This suggests a mechanism in

which mesityl oxide formation is limited by the surface reaction of two molecules of acetone, and the isobutene formation reaction is both promoted and inhibited by acetone on the surface.

Further information about the kinetics of acetone conversion to isobutene was obtained by measuring the initial rates of isobutene and mesityl oxide formation as a function of acetone and water partial pressure at 673 K and 723 K. The resulting data are shown in Figures 9 and 10. Figure 9 shows

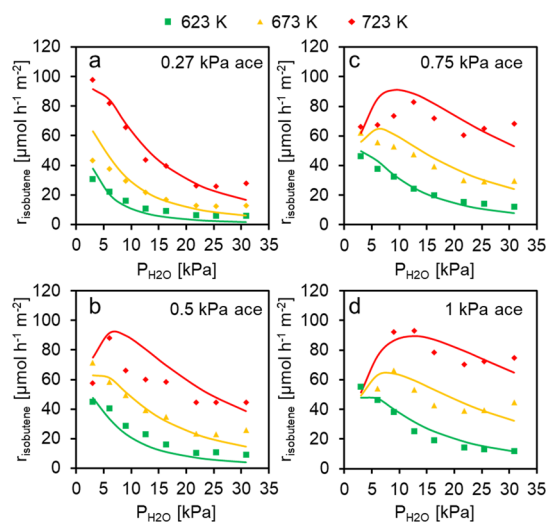


Figure 9. Rate of isobutene formation as function of temperature and reactant partial pressures. Reaction conditions: atmospheric pressure, 5.5 mg of $\text{Zn}_x\text{Zr}_y\text{O}_z$ (2.2 wt % Zn), 50 mL min^{-1} He, $X_{\text{acetone}} < 7\%$, (a) 0.27 kPa acetone, (b) 0.5 kPa acetone, (c) 0.75 kPa acetone, and (d) 1 kPa acetone. Solid lines represent a fit of eq 2 to the experimental data.

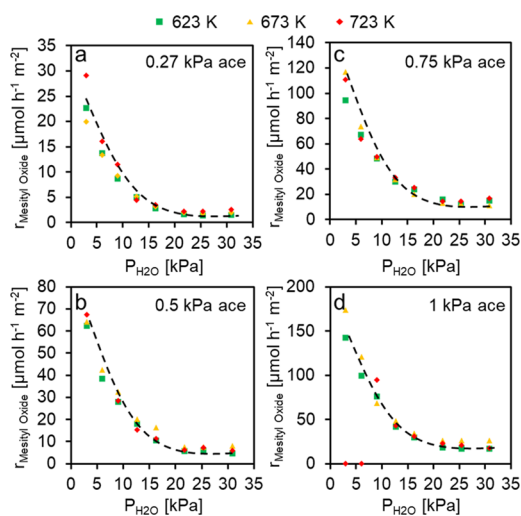


Figure 10. Rate of mesityl oxide formation as a function of temperature and reactant partial pressures. Reaction conditions: atmospheric pressure, 5.5 mg of $\text{Zn}_x\text{Zr}_y\text{O}_z$ (2.2 wt % Zn), 50 mL min^{-1} He, $X_{\text{acetone}} < 7\%$, (a) 0.27 kPa acetone, (b) 0.5 kPa acetone, (c) 0.75 kPa acetone, and (d) 1 kPa acetone. Dashed lines are a guide for the eye.

that rate of isobutene formation increases with increasing temperature. As the temperature increases, the inhibiting effects of water are less prominent, suggesting that the competitive adsorption of acetone and water on active sites

lies in favor of acetone at higher temperatures. Figure 10 shows that while the rate of mesityl oxide formation increases with increasing partial pressure of acetone, the rate of this reaction at a given partial pressure of acetone and water is nearly independent of the temperature between 623 and 723 K. The ratio of isobutene to mesityl oxide formed as a function of acetone and water partial pressure at 623, 673, and 723 K is presented in Figure 11. The selectivity toward isobutene increases with increasing water partial pressure and decreases with increasing acetone partial pressure, demonstrating that water inhibits mesityl oxide formation more than isobutene formation. The selectivity to isobutene relative to mesityl oxide also increases as temperature increases because the rates of mesityl oxide formation are relatively unaffected by temperature but the activation energy for isobutene formation is positive.

3.4.6. Proposed Mechanism and Kinetic Model for Acetone Conversion to Isobutene. Based on the measured kinetics and the proposed roles of acid and base sites for the reactions of acetone, diacetone alcohol, and mesityl oxide to isobutene, we propose the mechanism for the conversion of acetone to isobutene shown in Scheme 5. The first step is the coupling of acetone to form diacetone alcohol. The first acetone adsorbs onto a Lewis acid site, and a basic oxygen abstracts a hydrogen from one of the methyl groups. The second acetone adsorbs onto an adjacent acid site and is attacked by the carbanion, forming a C–C bond. A hydrogen cation is then added to the negatively charged oxygen, producing adsorbed diacetone alcohol.

There are several possible pathways for the formation of isobutene and acetic acid from adsorbed diacetone alcohol, as shown in Scheme 5. The first is the rightmost pathway shown in this scheme. Water adsorbs dissociatively and forms a temporary Brønsted acidic proton, which protonates the hydroxyl group of the adsorbed diacetone alcohol. Next, in a concerted step, the hydroxyl group that came from water adds to the carbonyl group while the C–C bond is broken to form isobutene, water, and acetic acid. In the second pathway, a variant of the first, diacetone alcohol adds a proton produced by heterolytic dissociation of water and then undergoes dehydration, leaving behind a carbocation intermediate. The next step is then the addition of a hydroxyl group, produced by the heterolytic dissociation of water, to the carbonyl group followed by C–C bond cleavage to produce isobutene and acetic acid. The third pathway (left) involves Lewis acid-catalyzed dehydration of diacetone alcohol to form mesityl oxide, which either desorbs from the surface or abstracts a hydrogen from the catalyst surface to produce the carbocation intermediate in the middle pathway. This intermediate then forms isobutene and acetic acid by addition of a hydroxyl group and cleavage of the C–C bond. In each of these three cases, the key transition state involves a partial bond between the hydroxyl group and the carbonyl, the breaking of a C–C bond, the formation of a C=C double bond, and a partial positive charge on the most substituted carbon. The acetic acid formed then undergoes further ketonization to produce more surface acetone, water, and CO_2 .

Two different rate expressions for the reaction kinetics were developed and fit to the experimental data. Equation 1 was derived for the case in which the rate-limiting step is C–C coupling of acetone to produce diacetone alcohol (labeled “a” on Scheme 5), and eq 2 was derived for the case in which the rate-limiting step is the decomposition of the C_6 intermediate

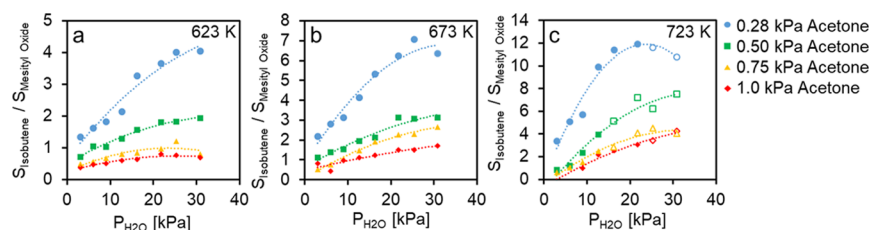
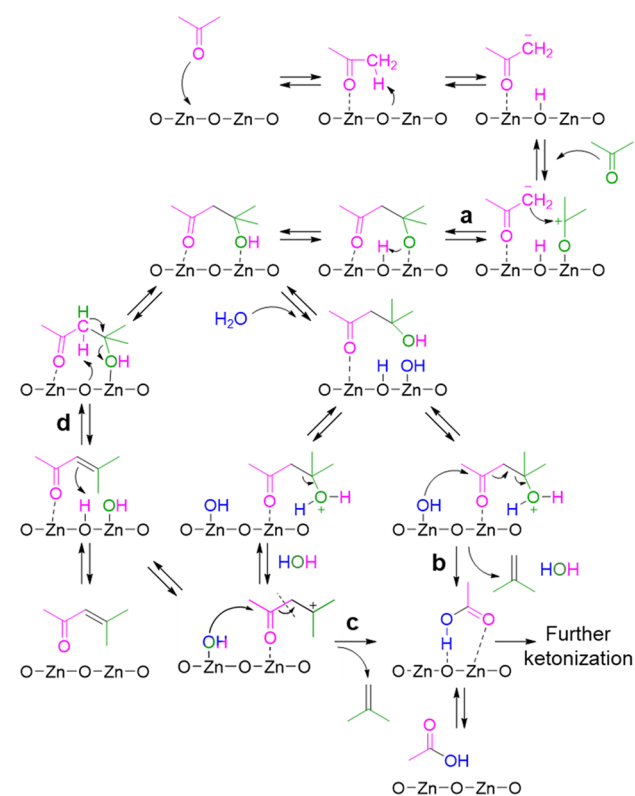


Figure 11. Selectivity ratio of isobutene to mesityl oxide (carbon %) as a function of temperature and partial pressure of reactants. Reaction conditions: atmospheric pressure, 5.5 mg of $\text{Zn}_x\text{Zr}_y\text{O}_z$ (2.2 wt % Zn), 50 mL min^{-1} He, $X_{\text{acetone}} < 7\%$, (a) 623, (b) 673, and (c) 723 K. Hollow data points represent initial rates measured for conditions that resulted in catalyst deactivation. Dashed lines are a guide for the eye.

Scheme 5. Proposed Mechanism for the Conversion of Acetone to Isobutene and Acetic Acid



(either protonated diacetone alcohol or a C_6 carbocation intermediate) to produce isobutene and acetic acid (labeled “b” or “c” on Scheme 5). The step marked “d” in Scheme 5 was not considered as a rate-limiting step for isobutene formation because no significant kinetic isotope effect was observed for deuterated acetone. The full derivations of these rate expressions based upon the elementary steps, assumptions, and site balances, as well as descriptions of the rate constants, are given in the Supporting Information. In eqs 1 and 2, given below, P_A and $P_{\text{H}_2\text{O}}$ are the partial pressures of acetone and water, respectively; k_1 and k_{-1} are the forward and reverse rate constants for the coupling of acetone to diacetone alcohol; K_A and $K_{\text{H}_2\text{O}}$ are the equilibrium constants for the adsorption of acetone and water onto active sites, respectively; k_2 is the rate constant for the dehydration of diacetone alcohol to produce mesityl oxide; and k_3 is the rate constant for the decomposition of diacetone alcohol to produce isobutene and acetic acid.

$$r_{\text{isobutene}} = \frac{k_1 K_A^2 P_A^2 - k_{-1} \left(\frac{k_1 K_A^2 P_A^2}{(k_{-1} + k_2 + k_3 P_{\text{H}_2\text{O}})} \right)}{(K_A P_A + K_{\text{H}_2\text{O}} P_{\text{H}_2\text{O}})^2} \quad (1)$$

$$r_{\text{isobutene}} = \frac{\frac{k_1 K_A^2 P_A^2 k_3 K_{\text{H}_2\text{O}} P_{\text{H}_2\text{O}}}{(k_{-1} + k_2 + k_3 P_{\text{H}_2\text{O}})}}{(K_A P_A + K_{\text{H}_2\text{O}} P_{\text{H}_2\text{O}})^3} \quad (2)$$

These equations were derived with the following assumptions: the adsorption and desorption of acetone and water are quasi-equilibrated; the ketonization of acetic acid is rapid; the pseudo-steady-state approximation can be applied to the rate of formation of diacetone alcohol; the surface is saturated with acetone and water; and the partial pressure of mesityl oxide is negligible (as rates of mesityl oxide formation become zero upon extrapolating to zero conversion). It should also be noted that the rate expression derived from eq 1 would be the same if mesityl oxide were an intermediate for isobutene formation because C–C bond formation would still be rate limiting.

Equations 1 and 2 were fit to the measured rate data taken as a function of temperature, partial pressure of H_2O , and partial pressure of acetone by adjusting the rate parameters to minimize the sum of the squares of the residuals. The form of eq 2 is a more accurate representation of the data, as evidenced by the parity plots shown in Figure 12, suggesting that the rate-

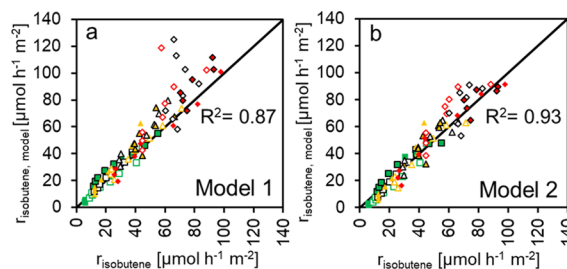


Figure 12. Parity plots for the rate of isobutene formation for (a) model 1 based upon eq 1 and (b) model 2 based upon eq 2. Green squares, 573 K; yellow triangles, 623 K; red diamonds, 673 K.

limiting step for isobutene formation is the decomposition of diacetone alcohol. The model for the case in which the rate of isobutene formation is limited by C–C coupling of diacetone alcohol fits well at low acetone partial pressures and low temperatures but breaks down at high temperatures and high partial pressures of acetone. This could be explained by the fact that, while water inhibits the reaction by occupying active sites, it is necessary to prevent deactivation and promote the decomposition of diacetone alcohol by providing surface hydroxyl groups and Brønsted acidic protons. This promoting role of water is not as captured in the first model. The rate

parameters obtained from the fit of the rate data to eq 2 are given in Table S2, and the Arrhenius plots are given in Figure S18. The resulting apparent activation energy for isobutene formation is $160 \pm 19 \text{ kJ mol}^{-1}$.

Based upon measurements of the reaction kinetics, the measured kinetic isotope effects, and the effect of the acid/base ratio on the kinetics of the acetone to isobutene conversion, we conclude that the acetone to isobutene reaction proceeds via C–C coupling to produce diacetone alcohol followed by protonation and concerted –OH addition and C–C bond cleavage to produce isobutene and acetic acid, which undergoes further condensation to produce acetone. Isobutene may also form via dehydration to mesityl oxide followed by hydrolysis of the addition product in a secondary pathway. As observed from the infrared spectra of adsorbed pyridine and the NH_3 TPD spectrum of $\text{Zn}_x\text{Zr}_y\text{O}_z$, significant quantities of Brønsted acid sites were not identified, suggesting that the Brønsted acidic protons involved in the reaction are generated from water during the reaction. DFT calculations reported by Sun et al. concluded that water dissociation occurs on Zn-modified ZrO_2 (111), and DRIFTS spectra of adsorbed D_2O acquired by the authors suggested that water dissociation occurs over ZrO_2 and $\text{Zn}_1\text{Zn}_{10}\text{O}_z$.¹⁶ Our model of the kinetics of isobutene formation from acetone, which involves the dissociative adsorption of water, is consistent with our experimental observation of the effects of water partial pressure on the kinetics.

In both pathways, the key transition state for isobutene formation from the C_6 intermediate involves the addition of a surface hydroxyl group to the carbonyl group as the C–C bond is broken. We find that the role of water for the conversion of acetone to isobutene is to prevent deactivation and inhibit acetone decomposition to methane and CO_2 , and we suggest that water dissociates to produce protons and hydroxyl groups that participate in the decomposition of the C_6 intermediates. The addition of water shifts the equilibrium toward diacetone alcohol and away from mesityl oxide, thereby preventing side-product formation and limiting the coupling of mesityl oxide with acetone to produce C_9 compounds, such as isophorone and mesitylene, which contribute to coke formation.

4. CONCLUSIONS

We have undertaken a comprehensive study of the reaction pathway, mechanism, and roles of acid and base sites for the reactions of ethanol and acetone to isobutene over $\text{Zn}_x\text{Zr}_y\text{O}_z$. An important finding is that the distribution of products formed is a strong function of the acid/base properties of the catalysts. Dispersion of zinc oxide on zirconia produces Zn–O–Zr moieties that exhibit Lewis basic sites weaker in base strength than those on ZnO, and Lewis acidic sites that are weak to moderate in strength. The ratio between Lewis acidic and Lewis basic sites depends on the amount of Zn dispersed on the surface of zirconia. A further consequence of dispersing zinc oxide on zirconia is the transformation of monoclinic ZrO_2 to the tetragonal phase.

The reaction of ethanol to isobutene proceeds via ethanol dehydrogenation to acetaldehyde, oxidation of acetaldehyde to acetic acid, and ketonization of acetic acid to acetone. While acetone is a key intermediate in the conversion of ethanol to isobutene, ethanol can also undergo dehydration to produce ethene, and acetone can decompose to form methane and CO_2 . The introduction of basicity on the surface of $\text{Zn}_x\text{Zr}_y\text{O}_z$ reduces the selectivity for ethanol conversion to ethene versus

to acetaldehyde (and thus acetone) and reduces the decomposition of acetone to CH_4 and CO_2 .

Since acetone is a key intermediate to the formation of isobutene from ethanol, we studied the mechanism and kinetics of this reaction in detail. Acetone undergoes condensation to diacetone alcohol on $\text{Zn}_x\text{Zr}_y\text{O}_z$. This product then forms mesityl oxide by dehydration and isobutene and acetic acid by decomposition. The acetic acid produced as a byproduct of the last reaction undergoes further ketonization to form acetone. The reaction of diacetone alcohol produces acetone as the principal product, indicating that the condensation of acetone to diacetone alcohol is reversible, consistent with the thermodynamics of this reaction. Measurements of the kinetic isotope effect for the reaction of acetone to isobutene suggest that the rate-limiting step is either the coupling of acetone to diacetone alcohol or the decomposition of diacetone alcohol. Modeling the effects of water and acetone partial pressure on the rate of isobutene formation over $\text{Zn}_x\text{Zr}_y\text{O}_z$ supports the conclusion that the rate-limiting step is the decomposition of diacetone alcohol. While water inhibits the rate of isobutene formation, it is necessary to hydrate the catalyst surface to promote the oxidation of acetaldehyde to acetic acid. The presence of water vapor also inhibits the dehydration of ethanol to ethene and diacetone alcohol to mesityl oxide, which forms condensation products that lead to coke formation and catalyst deactivation. A rate expression for the formation of isobutene from acetone developed from our understanding of the reaction mechanism is in good agreement with our observation of the effects of acetone and water partial pressures and of temperature.

Our studies reported in Section 3.3 indicate that successful conversion of ethanol to acetone over $\text{Zn}_x\text{Zr}_y\text{O}_z$ requires avoidance of ethanol dehydration. This reaction can be minimized at 698 K using $\text{S/C} = 5$ and high space times to promote the cascade reaction. Section 3.4 shows that optimal yields of isobutene from acetone over $\text{Zn}_x\text{Zr}_y\text{O}_z$ can be achieved at 723 K with $\text{S/C} = 5$, under which conditions the activity is high and the temperature is high enough to limit mesityl oxide formation but low enough to prevent acetone decomposition to methane and CO_2 as well as the formation of C_9 condensation products, which lead to coke formation. Ultimately, a two-step process in which ethanol is first converted to acetone at 698 K followed by acetone conversion to isobutene at 723 K could be employed to optimize yields of isobutene from ethanol. Overall, this study provides a clear sequence of reactions for the conversion of ethanol and acetone to isobutene over ZrO_2 , ZnO, and $\text{Zn}_x\text{Zr}_y\text{O}_z$. It also answers some key questions concerning the mechanism, site requirements, and role of water in the selective formation of isobutene from renewable platform molecules.

■ ASSOCIATED CONTENT

Supporting Information

The Supporting Information is available free of charge on the ACS Publications website at DOI: 10.1021/acscatal.9b03045.

Mechanism of propene formation from ethanol and acetone via MPV reduction (Scheme S1); supplemental catalyst characterization (ICP, DRIFTS-py, NH_3 -TPD, CO_2 -TPD) (Figures S1–S5, Table S1); gas-phase free energy of formation calculated from DFT (Figure S6); supplemental kinetic measurements (Figures S7–S17); kinetic parameters from model 2 (Table S2); Arrhenius

plots for rate constants given in Table S2 (Figure S18); and derivation of rate expressions (PDF)

AUTHOR INFORMATION

Corresponding Author

*E-mail: alexbell@berkeley.edu.

ORCID

F. Dean Toste: 0000-0001-8018-2198

Alexis T. Bell: 0000-0002-5738-4645

Notes

The authors declare no competing financial interest.

ACKNOWLEDGMENTS

This work was funded by the Director, Office of Science, Office of Basic Energy Sciences of the U.S. Department of Energy under contract no. DE-AC02-05CH11231. J.R. would also like to acknowledge funding from the National Science Foundation Graduate Research Fellowship (grant no. DGE 1106400). The authors thank Darinka Primc and Ezra Clark for assistance with the collection of Raman Spectra and SEM data, respectively. The authors also thank Christopher Ho for useful discussion and assistance with QChem calculations.

REFERENCES

- (1) Mascal, M. Chemicals from Biobutanol: Technologies and Markets. *Biofuels, Bioprod. Biorefin.* **2012**, *6*, 483–493.
- (2) Collignon, F.; Mariani, M.; Moreno, S.; Remy, M.; Poncelet, G. Gas Phase Synthesis of MTBE from Methanol and Isobutene over Dealuminated Zeolites. *J. Catal.* **1997**, *166*, 53–66.
- (3) Rorrer, J. E.; Bell, A. T.; Toste, F. D. Synthesis of Biomass-Derived Ethers for Use as Fuels and Lubricants. *ChemSusChem* **2019**, *12*, 2835–2858.
- (4) Bender, M. An Overview of Industrial Processes for the Production of Olefins - C₄ Hydrocarbons. *ChemBioEng Rev.* **2014**, *1*, 136–147.
- (5) Li, Y.; He, D.; Zhu, Q.; Zhang, X.; Xu, B. Effects of Redox Properties and Acid–Base Properties on Isosynthesis over ZrO₂-Based Catalysts. *J. Catal.* **2004**, *221*, 584–593.
- (6) Erkey, C.; Wang, J.; Postula, W.; Feng, Z.; Philip, C. V.; Akgerman, A.; Anthony, R. G. Isobutylene Production from Synthesis Gas over Zirconia in a Slurry Reactor. *Ind. Eng. Chem. Res.* **1995**, *34*, 1021–1026.
- (7) Tseng, S. C.; Jackson, N. B.; Ekerdt, J. G. Isosynthesis Reactions of CO₂ over Zirconium Dioxide. *J. Catal.* **1988**, *109*, 284–297.
- (8) Maruya, K.; Komiya, T.; Hayakawa, T.; Lu, L.; Yashima, M. Active Sites on ZrO₂ for the Formation of Isobutene from CO and H₂. *J. Mol. Catal. A: Chem.* **2000**, *159*, 97–102.
- (9) Chapman, L. Transport and Climate Change: A Review. *J. Transp. Geogr.* **2007**, *15*, 354–367.
- (10) Dagle, V. L.; Smith, C.; Flake, M.; Albrecht, K. O.; Gray, M. J.; Ramasamy, K. K.; Dagle, R. A. Integrated Process for the Catalytic Conversion of Biomass-Derived Syngas into Transportation Fuels. *Green Chem.* **2016**, *18*, 1880–1891.
- (11) Van Leeuwen, B. N. M.; Van Der Wulp, A. M.; Duijnste, I.; Van Maris, A. J. A.; Straathof, A. J. J. Fermentative Production of Isobutene. *Appl. Microbiol. Biotechnol.* **2012**, *93*, 1377–1387.
- (12) Qureshi, N.; Blaschek, H. P. Recent Advances in ABE Fermentation: Hyper-Butanol Producing Clostridium Beijerinckii BA₁₀₁. *J. Ind. Microbiol. Biotechnol.* **2001**, *27*, 287–291.
- (13) Sreekumar, S.; Baer, Z. C.; Pazhamalai, A.; Gunbas, G.; Grippo, A.; Blanch, H. W.; Clark, D. S.; Toste, F. D. Production of an Acetone-Butanol-Ethanol Mixture from Clostridium Acetobutylicum and Its Conversion to High-Value Biofuels. *Nat. Protoc.* **2015**, *10*, 528–537.

- (14) Kujawska, A.; Kujawski, J.; Bryjak, M.; Kujawski, W. ABE Fermentation Products Recovery methods—A Review. *Renewable Sustainable Energy Rev.* **2015**, *48*, 648–661.

- (15) Sun, J.; Zhu, K.; Gao, F.; Wang, C.; Liu, J.; Peden, C. H. F.; Wang, Y. Direct Conversion of Bio-Ethanol to Isobutene on Nanosized Zn_xZr_yO₂ Mixed Oxides with Balanced Acid-Base Sites. *J. Am. Chem. Soc.* **2011**, *133*, 11096–11099.

- (16) Sun, J.; Baylon, R. A. L.; Liu, C.; Mei, D.; Martin, K. J.; Venkatasubramanian, P.; Wang, Y. Key Roles of Lewis Acid–Base Pairs on Zn_xZr_yO₂ in Direct Ethanol/Acetone to Isobutene Conversion. *J. Am. Chem. Soc.* **2016**, *138*, 507–517.

- (17) Liu, C.; Sun, J.; Smith, C.; Wang, Y. A Study of Zn_xZr_yO₂ Mixed Oxides for Direct Conversion of Ethanol to Isobutene. *Appl. Catal., A* **2013**, *467*, 91–97.

- (18) Li, H.; Sun, J.; Wang, Y. Surface Acetone Reactions on Zn_xZr_yO₂: A DRIFTS-MS Study. *Appl. Catal., A* **2019**, *573*, 22–31.

- (19) Crisci, A. J.; Dou, H.; Prasomsri, T.; Román-Leshkov, Y. Cascade Reactions for the Continuous and Selective Production of Isobutene from Bioderived Acetic Acid Over Zinc-Zirconia Catalysts. *ACS Catal.* **2014**, *4*, 4196–4200.

- (20) Herrmann, S.; Iglesia, E. Selective Conversion of Acetone to Isobutene and Acetic Acid on Aluminosilicates: Kinetic Coupling between Acid-Catalyzed and Radical-Mediated Pathways. *J. Catal.* **2018**, *360*, 66–80.

- (21) Hutchings, G. J.; Johnston, P.; Lee, D. F.; Williams, C. D. Acetone Conversion to Isobutene in High Selectivity Using Zeolite β Catalyst. *Catal. Lett.* **1993**, *21*, 49–53.

- (22) Ponomareva, O. A.; Mal'tseva, A. A.; Maerle, A. A.; Rodionova, L. I.; Pavlov, V. S.; Dobryakova, I. V.; Belova, M. V.; Ivanova, I. I. Production of Isobutylene from Acetone over Micro – Mesoporous Catalysts. *Pet. Chem.* **2016**, *56*, 253–258.

- (23) Barton, D. G.; Soled, S. L.; Meitzner, G.D.; Fuentes, G. A.; Iglesia, E. Structural and Catalytic Characterization of Solid Acids Based on Zirconia Modified by Tungsten Oxide. *J. Catal.* **1999**, *181*, 57–72.

- (24) Rorrer, J.; He, Y.; Toste, F. D.; Bell, A. T. Mechanism and Kinetics of 1-Dodecanol Etherification over Tungstated Zirconia. *J. Catal.* **2017**, *354*, 13–23.

- (25) Rorrer, J.; Pindi, S.; Toste, F. D.; Bell, A. T. Effect of Alcohol Structure on the Kinetics of Etherification and Dehydration over Tungstated Zirconia. *ChemSusChem* **2018**, *11*, 3104–3111.

- (26) Zhao, B.; Men, Y.; Zhang, A.; Wang, J.; He, R.; An, W.; Li, S. Influence of Different Precursors on Isobutene Production from Bio-Ethanol over Bifunctional Zn₁Zr₁₀O_x Catalysts. *Appl. Catal., A* **2018**, *558*, 150–160.

- (27) Phadke, N. M.; Van Der Mynsbrugge, J.; Mansoor, E.; Getsoian, A. B.; Head-gordon, M.; Bell, A. T. Characterization of Isolated Ga³⁺ Cations in Ga/H-MFI Prepared by Vapor-Phase Exchange of H-MFI Zeolite with GaCl₃. *ACS Catal.* **2018**, *8*, 6106–6126.

- (28) Szulejko, J. E.; Kim, Y. H.; Kim, K. H. Method to Predict Gas Chromatographic Response Factors for the Trace-Level Analysis of Volatile Organic Compounds Based on the Effective Carbon Number Concept. *J. Sep. Sci.* **2013**, *36*, 3356–3365.

- (29) López, D. E.; Suwannakarn, K.; Bruce, D. A.; Goodwin, J. G., Jr. Esterification and Transesterification on Tungstated Zirconia: Effect of Calcination Temperature. *J. Catal.* **2007**, *247*, 43–50.

- (30) Zhao, Y.; Li, W.; Zhang, M.; Tao, K. A Comparison of Surface Acidic Features between Tetragonal and Monoclinic Nanostructured Zirconia. *Catal. Commun.* **2002**, *3*, 239–245.

- (31) Rao, G. S.; Rajan, N. P.; Pavankumar, V.; Chary, K. V. R. Vapor Phase Dehydration of Glycerol to Acrolein over NbOPO₄ Catalysts. *J. Chem. Technol. Biotechnol.* **2014**, *89*, 1890–1897.

- (32) Larsen, G.; Lotero, E.; Raghavan, S.; Parra, R. D.; Querini, C. A. A Study of Platinum Supported on Tungstated Zirconia Catalysts. *Appl. Catal., A* **1996**, *139*, 201–211.

- (33) Das, J.; Pradhan, S. K.; Sahu, D. R.; Mishra, D. K.; Sarangi, S. N.; Nayak, B. B.; Verma, S.; Roul, B. K. Micro-Raman and XPS Studies of Pure ZnO Ceramics. *Phys. B* **2010**, *405*, 2492–2497.

- (34) Dawood, F.; Schaak, R. E. ZnO-Templated Synthesis of Wurtzite-Type ZnS and ZnSe Nanoparticles. *J. Am. Chem. Soc.* **2009**, *131*, 424–425.
- (35) Rodriguez, J. A.; Wang, X.; Liu, G.; Hanson, J. C.; Hrbek, J.; Peden, C. H. F.; Iglesias-Juez, A.; Fernández-García, M. Physical and Chemical Properties of $Ce_{1-x}Zr_xO_2$ Nanoparticles and $Ce_{1-x}Zr_xO_2(111)$ Surfaces: Synchrotron-Based Studies. *J. Mol. Catal. A: Chem.* **2005**, *425*, 166–173.
- (36) Baylon, R. A. L.; Sun, J.; Kovarik, L.; Engelhard, M.; Li, H.; Winkelman, A. D.; Martin, K. J.; Wang, Y. Structural Identification of $Zn_xZr_yO_z$ Catalysts for Cascade Aldolization and Self-Deoxygenation Reactions. *Appl. Catal., B* **2018**, *234*, 337–346.
- (37) Li, M.; Feng, Z.; Xiong, G.; Ying, P.; Xin, Q.; Li, C. Phase Transformation in the Surface Region of Zirconia Detected by UV Raman Spectroscopy. *J. Phys. Chem. B* **2001**, *105*, 8107–8111.
- (38) Li, C.; Li, M. UV Raman Spectroscopic Study on the Phase Transformation of ZrO_2 , Y_2O_3 - ZrO_2 and SO_4^{2-}/ZrO_2 . *J. Raman Spectrosc.* **2002**, *33*, 301–308.
- (39) Kourieh, R.; Bennici, S.; Auroux, A. Acid and Redox Properties of Tungstated Zirconia Catalysts. *React. Kinet., Mech. Catal.* **2012**, *105*, 101–111.
- (40) Pokrovski, K.; Jung, K. T.; Bell, A. T. Investigation of CO and CO_2 Adsorption on Tetragonal and Monoclinic Zirconia. *Langmuir* **2001**, *4297*–4303.
- (41) Ma, Z.-Y.; Yang, C.; Wei, W.; Li, W.-H.; Sun, Y.-H. Surface Properties and CO Adsorption on Zirconia Polymorphs. *J. Mol. Catal. A: Chem.* **2005**, *227*, 119–124.
- (42) Kouva, S.; Honkala, K.; Lefferts, L.; Kanervo, J. Review: Monoclinic Zirconia, Its Surface Sites and Their Interaction with Carbon Monoxide. *Catal. Sci. Technol.* **2015**, *5*, 3473–3490.
- (43) Matheus, C. R. V.; Chagas, L. H.; Gonzalez, G. G.; Aguiar, E. F. S.; Appel, L. G. Synthesis of Propene from Ethanol: A Mechanistic Study. *ACS Catal.* **2018**, *7667*–7678.
- (44) Iwamoto, M. Selective Catalytic Conversion of Bio-Ethanol to Propene: A Review of Catalysts and Reaction Pathways. *Catal. Today* **2015**, *242*, 243–248.
- (45) Kostestkyy, P.; Yu, J.; Gorte, R. J.; Mpourmpakis, G. Structure–Activity Relationships on Metal-Oxides: Alcohol Dehydration. *Catal. Sci. Technol.* **2014**, *4*, 3861.
- (46) Xia, W.; Wang, F.; Mu, X.; Chen, K. Remarkably Enhanced Selectivity for Conversion of Ethanol to Propylene over ZrO_2 Catalysts. *Fuel Process. Technol.* **2017**, *166*, 140–145.
- (47) Chierigato, A.; Ochoa, J. V.; Bandinelli, C.; Fornasari, G.; Cavani, F.; Mella, M. On the Chemistry of Ethanol on Basic Oxides: Revising Mechanisms and Intermediates in the Lebedev and Guerbet Reactions. *ChemSusChem* **2015**, *8*, 377–388.
- (48) Ho, C. R.; Shylesh, S.; Bell, A. T. Mechanism and Kinetics of Ethanol Coupling to Butanol over Hydroxyapatite. *ACS Catal.* **2016**, *6*, 939–948.
- (49) Kang, M.; DeWilde, J. F.; Bhan, A. Kinetics and Mechanism of Alcohol Dehydration on γ - Al_2O_3 : Effects of Carbon Chain Length and Substitution. *ACS Catal.* **2015**, *5*, 602–612.
- (50) DeWilde, J. F.; Chiang, H.; Hickman, D. A.; Ho, C. R.; Bhan, A. Kinetics and Mechanism of Ethanol Dehydration on γ - Al_2O_3 : The Critical Role of Dimer Inhibition. *ACS Catal.* **2013**, *3*, 798–807.
- (51) Fan, D.; Dai, D.-J.; Wu, H.-S. Ethylene Formation by Catalytic Dehydration of Ethanol with Industrial Considerations. *Materials* **2013**, *6*, 101–115.
- (52) Eagan, N. M.; Kumbhalkar, M. D.; Buchanan, J. S.; Dumesic, J. A.; Huber, G. W. Chemistries and Processes for the Conversion of Ethanol into Middle-Distillate Fuels. *Nat. Rev. Chem.* **2019**, *3*, 223–249.
- (53) Vohs, J. M.; Barteau, M. A. Dehydration and Dehydrogenation of Ethanol and 1-Propanol on the Polar Surfaces of Zinc Oxide. *Surf. Sci.* **1989**, *221*, 590–608.
- (54) Nakajima, T.; Tanabe, K.; Yamaguchi, T.; Matsuzaki, I.; Mishima, S. Conversion of Ethanol to Acetone over Zinc Oxide-Calcium Oxide catalyst Optimization of Catalyst Preparation and Reaction Conditions and Deduction of Reaction Mechanism. *Appl. Catal.* **1989**, *52*, 237–248.
- (55) Rahman, M. M.; Davidson, S. D.; Sun, J.; Wang, Y. Effect of Water on Ethanol Conversion over ZnO. *Top. Catal.* **2016**, *59*, 37–45.
- (56) Silva-Calpa, L. del R.; Zonetti, P. C.; Rodrigues, C. P.; Alves, O. C.; Appel, L. G.; de Avillez, R. R. The $Zn_xZr_{1-x}O_{2-y}$ Solid Solution on m- ZrO_2 : Creating O Vacancies and Improving the m- ZrO_2 Redox Properties. *J. Mol. Catal. A: Chem.* **2016**, *425*, 166–173.
- (57) Silva-Calpa, L. d. R.; Zonetti, P. C.; de Oliveira, D. C.; de Avillez, R. R.; Appel, L. G. Acetone from Ethanol Employing $Zn_xZr_{1-x}O_{2-y}$. *Catal. Today* **2017**, *289*, 264–272.
- (58) Pala, R. G. S.; Metiu, H. Modification of the Oxidative Power of ZnO(10 $\bar{1}$ 0) Surface by Substituting Some Surface Zn Atoms with Other Metals. *J. Phys. Chem. C* **2007**, *111*, 8617–8622.
- (59) McFarland, E. W.; Metiu, H. Catalysis by Doped Oxides. *Chem. Rev.* **2013**, *113*, 4391–4427.
- (60) Chen, B.; Ma, Y.; Ding, L.; Xu, L.; Wu, Z.; Yuan, Q.; Huang, W. Reactivity of Hydroxyls and Water on a $CeO_2(111)$ Thin Film Surface: The Role of Oxygen Vacancy. *J. Phys. Chem. C* **2013**, *117*, 5800–5810.
- (61) Chenu, E.; Jacobs, G.; Crawford, A. C.; Keogh, R. A.; Patterson, P. M.; Sparks, D. E.; Davis, B. H. Water-Gas Shift: An Examination of Pt Promoted MgO and Tetragonal and Monoclinic ZrO_2 by in Situ Drifts. *Appl. Catal., B* **2005**, *59*, 45–56.
- (62) Wang, Y.; Muhler, M.; Wöll, C. Spectroscopic Evidence for the Partial Dissociation of H_2O on ZnO(10 $\bar{1}$ 0). *Phys. Chem. Chem. Phys.* **2006**, *8*, 1521–1524.
- (63) Pham, T. N.; Sooknoi, T.; Crossley, S. P.; Resasco, D. E. Ketonization of Carboxylic Acids: Mechanisms, Catalysts, and Implications for Biomass Conversion. *ACS Catal.* **2013**, *3*, 2456–2473.
- (64) Wang, S.; Iglesia, E. Experimental and Theoretical Assessment of the Mechanism and Site Requirements for Ketonization of Carboxylic Acids on Oxides. *J. Catal.* **2017**, *345*, 183–206.
- (65) Gumidyala, A.; Sooknoi, T.; Crossley, S. Selective Ketonization of Acetic Acid over HZSM-5: The Importance of Acyl Species and the Influence of Water. *J. Catal.* **2016**, *340*, 76–84.
- (66) Gangadharan, A.; Shen, M.; Sooknoi, T.; Resasco, D. E.; Mallinson, R. G. Condensation Reactions of Propanal over $Ce_xZr_{1-x}O_2$ Mixed Oxide Catalysts. *Appl. Catal., A* **2010**, *385*, 80–91.
- (67) Tosoni, S.; Pacchioni, G. Acetic Acid Ketonization on Tetragonal Zirconia: Role of Surface Reduction. *J. Catal.* **2016**, *344*, 465–473.
- (68) Fu, Y.; Zhang, L.; Yue, B.; Chen, X.; He, H. Simultaneous Characterization of Solid Acidity and Basicity of Metal Oxide Catalysts via the Solid-State NMR Technique. *J. Phys. Chem. C* **2018**, *24094*.
- (69) Zaki, M. I.; Hasan, M. A.; Pasupulety, L. Surface Reactions of Acetone on Al_2O_3 , TiO_2 , ZrO_2 , and CeO_2 : IR Spectroscopic Assessment of Impacts of the Surface Acid-Base Properties. *Langmuir* **2001**, *17*, 768–774.
- (70) Biaglow, A. I.; Sepa, J.; Gorte, R. J.; White, D. A ^{13}C NMR Study of the Condensation Chemistry of Acetone and Acetaldehyde Adsorbed at the Brønsted Acid Sites in H-ZSM-5. *J. Catal.* **1995**, *151*, 373–384.
- (71) Xu, T.; Munson, E. J.; Haw, J. F. Toward a Systematic Chemistry of Organic Reactions in Zeolites: In Situ NMR Studies of Ketones. *J. Am. Chem. Soc.* **1994**, *116*, 1962–1972.
- (72) Takanabe, K.; Aika, K.; Seshan, K.; Lefferts, L. Catalyst Deactivation during Steam Reforming of Acetic Acid over Pt/ ZrO_2 . *Chem. Eng. J.* **2006**, *120*, 133–137.